

CHARGE DENSITY WAVE TRANSITIONS IN THE  
TRANSITION METAL DICHALCOGENIDES

by

Gary K. Scott

B.Sc., University of California at Los Angeles, 1969

M.Sc., University of Washington, 1972

A THESIS SUBMITTED IN PARTIAL FULFILLMENT  
OF THE REQUIREMENTS FOR THE DEGREE OF

DOCTOR OF PHILOSOPHY

in the Department

of

Physics

Gary K. Scott 1981

SIMON FRASER UNIVERSITY

July 1981

All rights reserved. This thesis may not be  
reproduced in whole or in part, by photocopy  
or other means, without permission of the author.

APPROVAL

Name: Gary K. Scott  
Degree: Doctor of Philosophy  
Title of Thesis: Charge Density Wave Transitions  
in the Transition Metal  
Dichalcogenides

Examining Committee:

Chairman: M. Plischke

---

A.S. Arrott  
Supervisor

---

T.M. Rice

---

K.S. Viswanathan

---

J.C. Irwin

---

B. Bergersen  
External Examiner  
Associate Professor  
Department of Physics  
University of British Columbia

Date Approved: July 17, 1981

PARTIAL COPYRIGHT LICENSE

I hereby grant to Simon Fraser University the right to lend my thesis, project or extended essay (the title of which is shown below) to users of the Simon Fraser University Library, and to make partial or single copies only for such users or in response to a request from the library of any other university, or other educational institution, on its own behalf or for one of its users. I further agree that permission for multiple copying of this work for scholarly purposes may be granted by me or the Dean of Graduate Studies. It is understood that copying or publication of this work for financial gain shall not be allowed without my written permission.

Title of Thesis/Project/Extended Essay

Charge Density Wave Transition in the  
2H Transition Metal Dichalcogenides

Author:

(signature)

Gary K. Scott

(name)

April 21 1983

(date)

ABSTRACT

A microscopic Hamiltonian descriptive of the charge density wave (C.D.W.) transitions occurring in the 2H transition metal dichalcogenides is presented. From existing band structure calculations of these highly two dimensional compounds, the essential electronic feature is proposed to be the six equivalent  $\Gamma$ -K saddle points of the conduction band which in the two dimensional limit produce a logarithmic Van Hove type contribution to the density of states. Incorporation of lattice dynamical effects into the model Hamiltonian begins with the six equivalent longitudinal acoustic A symmetric phonons belonging to the star  $q=\pm G_i/3$ , observed to partially soften as the C.D.W. transition is approached from above.

With the C.D.W. active portions of the electronic conduction band and phonon Brillouin zone characterized, the model Hamiltonian, incorporating both electron-phonon and anharmonic interactions, is diagonalized in terms of the static lattice distortion amplitude, the order parameter appropriate to the C.D.W. phase. The C.D.W. electronic and phonon energy spectrum resulting from the diagonalization process are used to calculate, via numerical methods, the thermodynamical properties of the C.D.W. phase transition.

Taken as a whole, the results strongly support the model of  $\Gamma$ -K saddle points coupled through the C.D.W. distortion

amplitudes. Correlating the observed ratio of zero temperature electronic gap to lattice distortion with the observed partial softening of the  $q=\pm G_i/3$  longitudinal acoustic A symmetric phonons, a susceptibility difference comparing favorably with experiment is predicted. Also, the electronic saddle point model suggests a Fermi surface consistent with the de Haas-van Alpen results.

Finally, the temperature dependence of the six A symmetric modes in the C.D.W. phase, where they couple to form optically active Raman modes, is given and shown to conform well with experimental results.

ACKNOWLEDGEMENTS

Many diverse efforts were responsible for this thesis coming to a fruitful end. Foremost, I am grateful to Maurice Rice whose conception of the essential argument of this thesis and sustained critical guidance were invaluable. His perception of the relevant physics shaped and directed much of my effort while his continual commitment was instrumental to the final completion of this work.

Also, inestimable as a quickening force was Anthony Arrott. Able to discern the wheat from the shaft at a glance, he infused the daily task with inspirations.

Indebtedness to Jo-Ann Murphy whose nimble typing skills produced the final manuscript is sincerely acknowledged. Also, deep appreciation goes to Shyamal Bose whose meticulous editing formed a vital contribution to this thesis.

Finally, grateful acknowledgement is extended to the Simon Fraser Physics Department and the Natural Sciences and Engineering Research Council for their financial support during this undertaking.

TABLE OF CONTENTS

	<u>Page</u>
Approval Page .....	ii
Abstract .....	iii
Acknowledgements .....	v
Table of Contents .....	vi
List of Tables .....	viii
List of Figures .....	ix
CHAPTER 1 INTRODUCTION .....	1
1.1 Charge Density Wave Transitions in the Layered Metal Dichalcogenides .....	1
1.2 Structural and Electronic Properties of the 1T and 2H Polymorphs .....	2
1.3 Experiments Elucidating the C.D.W. State .....	7
CHAPTER 2 FORUMULATION OF C.D.W. Hamiltonian .....	15
2.1 C.D.W. Hamiltonian .....	15
2.2 Solution of C.D.W. Hamiltonian .....	22
2.3 C.D.W. Brillouin Zone .....	29
2.3A Electronic Brillouin Zone .....	29
2.3B Phonon Brillouin Zone .....	33
CHAPTER 3 THERMODYNAMICS .....	40
3.1 Free Energy Structure .....	40
3.2 Saddle Point Model .....	46
3.3 Phonon Free Energy .....	48

	<u>Page</u>
CHAPTER 4 NUMERICAL RESULTS OF SADDLE POINT MODEL ..	54
4.1 Parameters of C.D.W. State .....	54
4.2 Method of Calculation.....	60
4.3 Numerical Results .....	62
CHAPTER 5 CONCLUSIONS .....	74
5.1 Fermi Surface Topology .....	74
5.2 The Raman Active C.D.W. Modes.....	79
Appendix A .....	82
References .....	93



LIST OF TABLES

<u>Table</u>		<u>Page</u>
4.1	Electronic Susceptibility .....	72
4.2	Specific Heat Discontinuity .....	73

LIST OF FIGURES

<u>Figure</u>		<u>Page</u>
1.1	Resistivity of 1T and 2H Polymorphs vs. Temperature .....	11
1.2	Susceptibility of 1T and 2H Polymorphs vs. Temperature .....	11
1.3	Fermi Surface of 1T and 2H Polymorphs .....	12
1.4	Band Structure and Density of States for 1T and 2H TaSe <sub>2</sub> .....	13
1.5	Lattice Distortion Amplitude for 2H TaSe <sub>2</sub> and 2H NbSe <sub>2</sub> .....	14
2.1	L.A. (A) Phonon Dispersion along $\Gamma/M$ .....	39
3.1	G/3 Remapping of Full 2H Brillouin zone .....	52
3.2a	Position of Coupling $\Gamma/K$ Saddle Points .....	53
3.2b	Superposition of Coupling Saddle Points .....	53
4.1	G/3 Normal State Susceptibility .....	67
4.2	Zero Temperature Electronic Gap vs. Coupling Parameter .....	68
4.3	Electronic Gap vs. Temperature for $W_0 = 0$ .....	69
4.4	Electronic Gap Vs. Temperature for $W_0 = .1$ .....	70
4.5	Susceptibility of Normal and C.D.W. State .....	71
5.1	G/3 Remapping of Full 2H Brillouin Zone with C.D.W. Modification .....	80

<u>Figure</u>		<u>Page</u>
5.2a	Experimental C.D.W. Mode Frequencies .....	81
5.2b	Theoretical C.D.W. Mode Frequencies .....	81

CHAPTER 1  
INTRODUCTION

1.1 Charge Density Wave Transitions in the Layered Metal Dichalcogenides

A remarkable class of displacive phase transitions exist in a large number of the group VB transition metal dichalcogenides.<sup>1</sup> Now realized as a manifestation of electron-phonon coupling enhanced by the two dimensional environment existing in these layered compounds, these transitions were first interpreted by Wilson et al<sup>1</sup> where, using electron diffraction, the emergence of superlattice reflections about the parent Bragg points at sufficiently low temperature indicated new components to both the lattice and electronic periodicity. In addition to the simultaneous appearance of these charge density waves (C.D.W.) and periodic lattice distortions (P.L.D.) at the transition temperature, abrupt changes in the resistivity, magnetic susceptibility and specific heat were also observed.<sup>1</sup>

Chemically based on the composition  $\text{MX}_2$  where M is vanadium, niobium or tantalum and X is sulfur, selenium or tellurium, the transition metal dichalcogenides are structurally based upon a sandwiching format where hexagonally ordered planes of metal atoms are coordinated from above and below by hexagonally ordered chalcogen planes. Only relatively weak Van de Waals forces couple one X-M-X unit to the next.

In many respects, the C.D.W. transition occurring on the transition metal dichalcogenides is a two dimensional realization of the electronic/lattice instability initially envisioned by Peierls<sup>2</sup> and Fröhlich<sup>3</sup> as the mechanism which would necessarily drive a one dimensional metal to the insulating state by the introduction of an electronic gap at the Fermi surface, a result of the splitting of electronic states,  $\epsilon_{k-k_f}$  and  $\epsilon_{k+k_f}$  by coupling to a lattice distortion of  $2k_f$ . It is the special circumstance of one dimension, where the Fermi surface consists of the two points  $-k_f$  and  $k_f$ , that ensures that, below some temperature, the gain in electronic energy will dominate the positive lattice distortion energy and a C.D.W., indicative of the new periodicity at  $2k_f$ , will manifest itself. However, for higher dimensions, the criterion for a C.D.W. transition is a complex issue with such causative agents as Fermi surface topology, density of states structure and electron-phonon coupling strength assuming key roles<sup>10</sup>.

## 1.2 Structural and Electronic Properties of the 1T and 2H Polymorphs

Depending upon the alignment of the two chalcogen sheets which sandwich the transition metal, two basic polymorphs are possible, octahedral or trigonal prismatic. In the octahedral or 1T configuration, the chalcogen sheets differ by a 60 degree rotation about an axis perpendicular to the sheets and passing through the transition metal (c-axis) and thus assume a staggered

arrangement with one  $\text{MX}_2$  unit per unit cell. In the trigonal prismatic or 2H configuration, the chalcogens of a given sandwich align with each other but the successive sandwiches stacked with 60 degrees relative rotation about the c-axis and thus contain two  $\text{MX}_2$  units per unit cell.

This layered format results in a large anisotropy between basal plane and c-axis directions and thus renders these compounds highly two dimensional. For example, in both 1T and 2H polymorphs, the ratio of basal plane to c-axis resistivity is approximately 30.

Despite their structural similarity, the 1T and 2H polymorphs exhibit strikingly different properties in the C.D.W. state. For example, in 1T  $\text{TaSe}_2$ , entry into the C.D.W. state at 476K produces an almost order of magnitude discontinuous increase in resistivity, from  $5 \times 10^{-4}$  ohm-cm to  $1.5 \times 10^{-3}$  ohm-cm, while in 2H  $\text{TaSe}_2$ , only the slope of the resistivity changes at the transition temperature with the C.D.W. state displaying a greater conductivity than the normal state. Figures 1.1 and 1.2 clearly correlates this contrasting C.D.W. transition behavior with polymorphic form.

To understand these and other salient distinctions between the C.D.W. transitions in the 1T and 2H polymorphs, recourse to an intensive body of band structure calculations is fortunately available<sup>4</sup>.

Beginning with Wilson and Yoffe<sup>5</sup>, simple tight-binding arguments were employed to systematically interpret an extensive portion of the observed optical and electrical properties of the group IVB, VB and VIB transition metal dichalcogenides. The valence band (bonding band) consists of six broad bands ( $\sim 5\text{eV}$ ) derived primarily from the chalcogen p-orbitals, with each chalcogen supplying three p-orbits. As each chalcogen has four p-electrons, the remaining four electrons needed for a filled valence band are supplied by the transition metal, two from n-level s-electrons and two from (n-1) level d-electrons. Within this admittedly naive bonding picture, the conduction band (antibonding band) consists of three bands derived from the metal n-level s-orbital and two (n-1) level d-orbitals. The remaining three (n-1) level metal d-orbitals comprise the "non-bonding" manifold, situated within the  $\sim 6\text{eV}$  gap between the valence and conduction band and, as will be seen, are the source of C.D.W. activity.

Within the tight-binding context, the essential electronic characteristics of the group IVB, VB and VIB transition metal dichalcogenides can be explained. Starting with group IVB compounds, its two d-electrons are involved in the valence band and are thus semiconductors. Group VB compounds, with three d-electrons, are metallic as the extra single d-electron only partially fills the nonbonding band. Group VIB, as a result of hybridization effects<sup>6</sup> within the nonbonding manifold splits off a single lower band, is semiconducting as its two nonbonding

d-electrons fill the lower nonbonding band.

The APW calculations of Mattheiss<sup>6</sup>, elucidated the fine structure of the nonbonding manifold which is instrumental to the C.D.W. transition. The influence of octahedral as opposed to trigonal symmetry upon the three bands of the nonbonding manifold is drastic though the location and widths of the valence and conduction band remain essentially independent of polymorphic form.

In the octahedral situation, the character of the non-bonding manifold is basically that of three triply degenerate bands of d-symmetry with no hybridizing influences from either conduction or valence band states. The bandwidth is large, of the order of 4 eV and displays a relatively flat density of states, indicative of its two dimensional nature. Using a directed orbital approach Inglesfield<sup>7</sup> attributes the large band width to the strong overlap between the highly directed orbital lobes on adjacent metal atoms.

By contrast, in the trigonal prismatic coordination, extensive hybridization between the three nonbonding bands results in a  $\sim 1.3$  eV gap opening in this manifold with a single lower band and a merging of the upper two bands into the bottom of the conduction band. With the symmetry of  $d_{z^2}$  at  $\Gamma$ , this lower band, by virtue of the hybridization process, is quite narrow, of the order of  $\sim 1$  eV. Also, since the 2H polymorph contains two  $\text{MX}_2$  units per unit cell, the added complication of all bands being double sheeted must be borne in mind.



Figures 1.3 and 1.4 display the essential electronic and Fermi surface features of the 1T and 2H polymorphs as gleaned from a number of authors<sup>4,6,8</sup>.

In the 1T configuration the nesting Fermi surface model, initially developed by Chan and Heine<sup>10</sup> and involving coupling large portions of the Fermi surface by a single wavevector, appears applicable. A wavevector spanning either the ellipsoidal electron pocket across  $\Gamma$ -M ( $q \sim .58G$ , where  $G$  is a basal plane reciprocal lattice vector) or self-spanning of the electron pockets ( $q \sim G - .58G$ ) provides effective coupling of the Fermi surfaces. Experimentally, the abrupt increase in resistivity indicates substantial loss of Fermi surface. Also, doping experiments<sup>1</sup> indicate that Fermi surface geometry dictates the C.D.W. wavevector.

By contrast the 2H Fermi surface offers no readily discernible nesting mechanism<sup>8</sup>. An alternative model<sup>9</sup> for the C.D.W. transitions in the 2H compounds implicates the large density of states in the vicinity of the Fermi surface as the causal electronic agent. This peak is derived from the saddle points occurring approximately 1/2 to 2/3 out from  $\Gamma$  towards  $K$ , which would contribute a logarithmic singularity, in the two dimensional limit, to the total density of states.

A major concern of this thesis are model calculations of the C.D.W. state using the saddle point description to parameterize the electronic Brillouin zone of the normal state.

### 1.3 Experiments Elucidating the C.D.W. State

The work of Wilson et al<sup>1</sup> was of fundamental importance in establishing the C.D.W. interpretation to the displacive transitions observed in the transition metal dichalcogenides. In addition to a wealth of new results derived primarily from electron diffraction, they presented resolution within the C.D.W. formulation of previously anomalous magnetic, electrical and optical data.

With the neutron scattering experiments of Moncton, Axe and Di Salvo<sup>13</sup>, progressive enhancement of the "Kohn-like" anomaly in the L.A.(A) phonon branch, characterization of soft mode behavior, was observed in  $2H TaSe_2$  and  $2H NbSe_2$  as the C.D.W. transition was approached from above. Though the phonon frequency remained finite at the transition temperature, the static lattice displacements of the C.D.W. state are essentially derived from the normal mode displacements of the L.A.(A) phonon.

Also, with the resolution offered by neutron diffraction, Moncton et al<sup>13</sup> were able to detect slight modification of the C.D.W. wavevector with temperature. The electron diffraction studies of Wilson et al<sup>1</sup> had initially indicated a C.D.W. periodicity of approximately  $G_i/3$ ,  $G_i$  being any of the three symmetry equivalent basal plane reciprocal lattice vectors of the

normal state. However, working with  $2H TaSe_2$  the neutron studies revealed progressive alteration of the C.D.W. wave-vector from a slightly incommensurate value of  $q_0 = G_i/3 \cdot (1+.02)$  at the normal incommensurate phase transition of  $T_c = 120K$  to a commensurate value of  $q_0 = G_i/3$  reached at a transition temperature of  $T_{Ic} = 95K$ .

Existing as an integral fraction of the lattice periodicity, a commensurate C.D.W. state retains the property of lattice translational invariance while in the more general incommensurate situation where lattice and C.D.W. periodicity have no integral relationship, translational invariance is lost. With departure from commensurability as a small effect, this thesis will treat the  $2H$  C.D.W. transition in the purely commensurate context. As Figure 1.5 illustrates, entry into the commensurate state from the incommensurate state as the temperature is lowered manifests itself only as a slight modification of the C.D.W. distortion amplitude.

Though establishing the essential lattice dynamics associated with the C.D.W. transition, the neutron work of Moncton et al<sup>13</sup> was not decisive enough to distinguish the explicit symmetry of the C.D.W. configuration. This was achieved by Holy et al<sup>15</sup> where the observed Raman spectrum of the C.D.W. phonons and attending selection rules corroborated with the existence of an inversion symmetric three-C.D.W. state. The temperature dependence of the C.D.W. phonons,

more completely documented by Steigmeier et al<sup>22</sup>, revealed softening and broadening as the transition temperature was approached from below but, as with the neutron data<sup>13</sup> no mode was observed to go completely soft.

Regarding the C.D.W. influence on electronic properties, Barker et al<sup>20</sup>, using infrared reflectivity, concluded the existence of gap formation at  $\sim .3$  eV in the C.D.W. state of  $2H TaSe_2$ . The possibility of further structure below .05 eV, the lower end of the investigated energy range, exists as the conductivity, extracted from the reflectivity by Kramers-Kronig analysis, extrapolated to a dc value significantly below that experimentally observed.

The de Haas-Van Alphen measurements on the C.D.W. state of  $2H TaSe_2$  by Graebner<sup>18</sup> reveals 8 orbits with magnetic field parallel to the c-axis. As the Fermi surface for the  $2H$  configuration is composed of two sheets, a consequence of there being two  $MX_2$  sandwiches per unit cell, with topologies equivalent except for differences arising through the relatively weak interlayer interaction, the dHvA data is consistent with the grouping of the orbits into two similar sets of four orbits each. Tilting the magnetic field away from the c-axis increases the effective radius of all orbits, a result reflecting the topology of the parent undistorted Fermi surface, characterized by essentially cylindrical sections centered

about  $\Gamma$  and the six K points and running parallel to the c-axis. In Chapter 5, an explanation of these results will be proposed within the context of the saddle point model.

Finally, the specific heat and resistivity results of Craven et al<sup>21</sup> for  $2H TaSe_2$  and  $2H TaS_2$  in the vicinity of the C.D.W. transition provided sensitive measurement of these quantities. With the influence of critical fluctuation clearly evident, the excess specific heat above the mean field estimate for temperature just above the transition temperature were used to provide a determination of the zero temperature coherence length  $\xi_0$ . Results indicated a coherence length  $\xi_0 < 10\text{\AA}$ . This short coherence length, as McMillan<sup>11</sup> suggested, tends to implicate phonons, rather than electrons, as the major entropy source driving the C.D.W. transition.

In subsequent chapters, a Hamiltonian incorporating both electronic and lattice influences will be developed which satisfactorily explains a major portion of the diverse body of C.D.W. experimental data in the layered transition metal dichalcogenides.

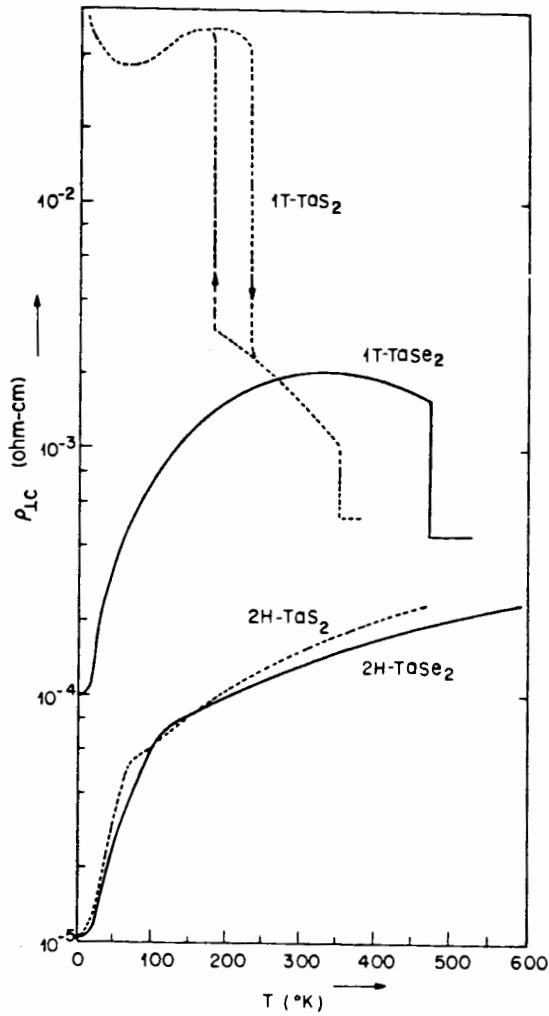


Fig. 1.1: Resistivity in the basal plane for various 1T and 2H polymorphs. The contrasting behavior of these two polymorphs indicates a different C.D.W. mechanism operating in each situation. From ref. 1

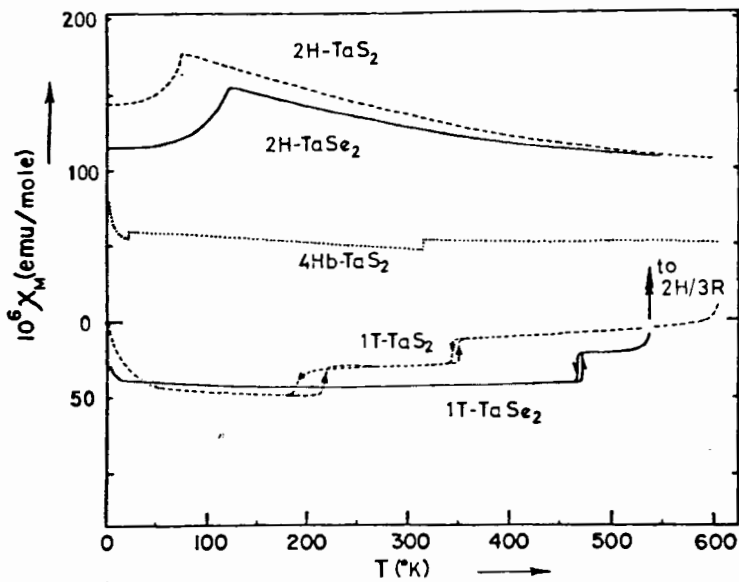

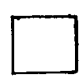


Fig. 1.2: Susceptibility for various 1T and 2H polymorphs. The decrease in susceptibility in the C.D.W. state indicates loss of free carriers in both 1T and 2H situations.

 Electron  
 Hole

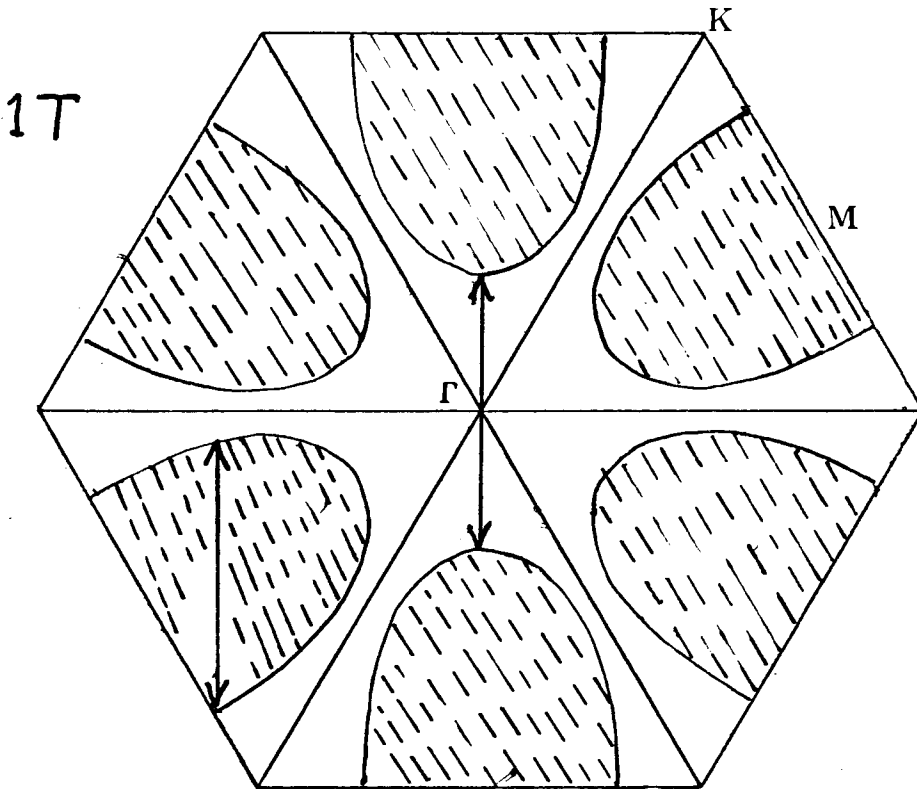
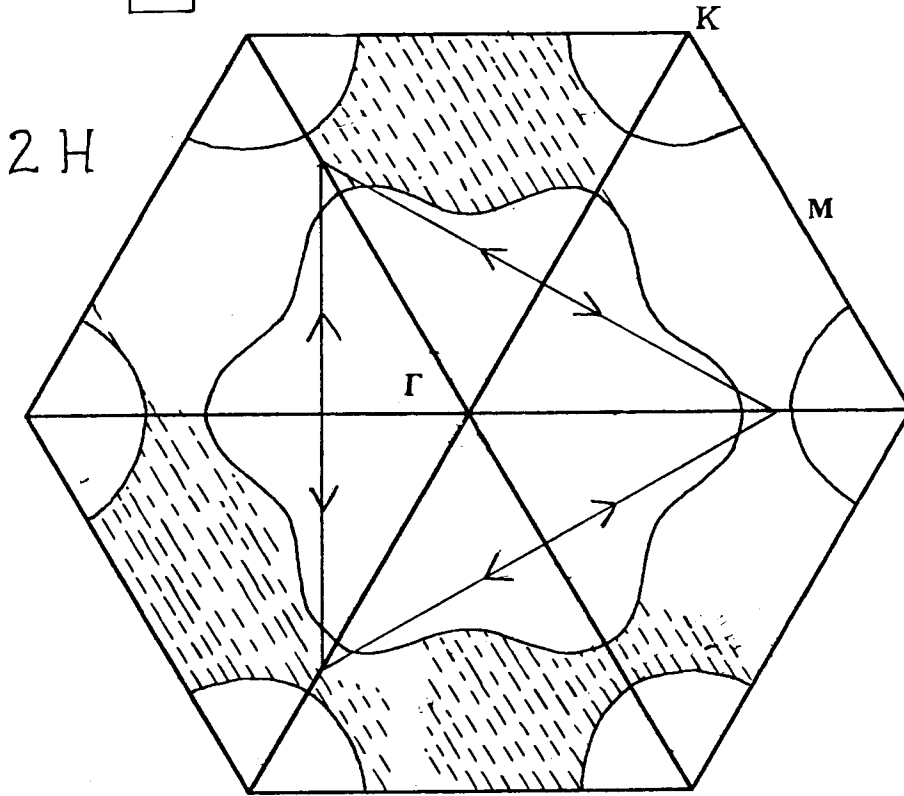


Fig. 1.3: Qualitative display of the Fermi surface for the 1T and 2H configuration. Arrows in the 2H diagram couple  $\Gamma/K$  saddle points while arrows in the 1T diagram span the M-point hole pockets. These regions are the electronic area of C.D.W. activity.

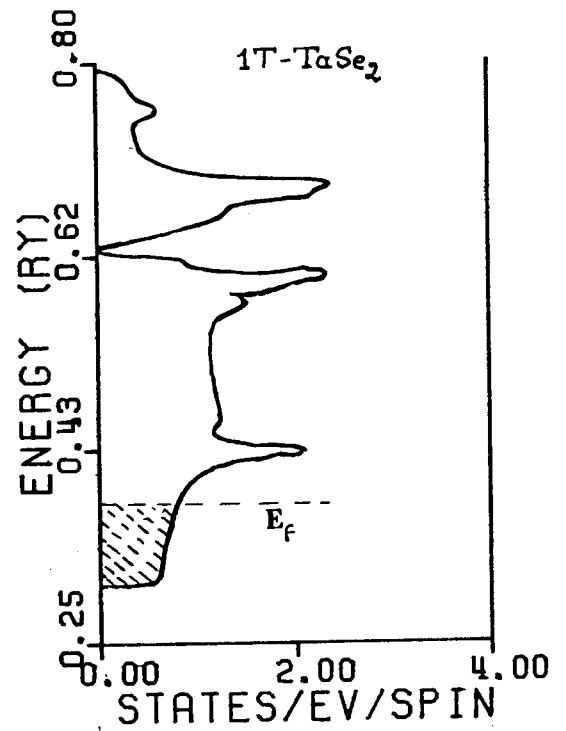
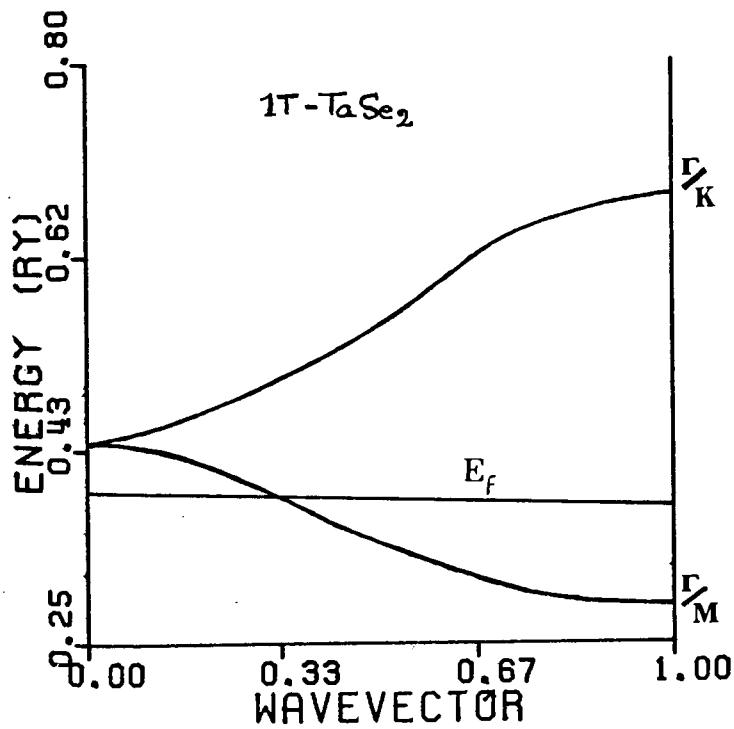
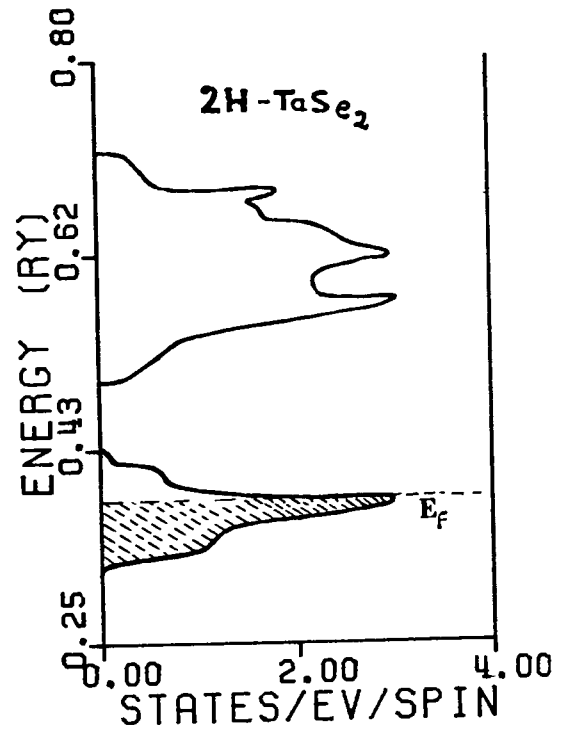
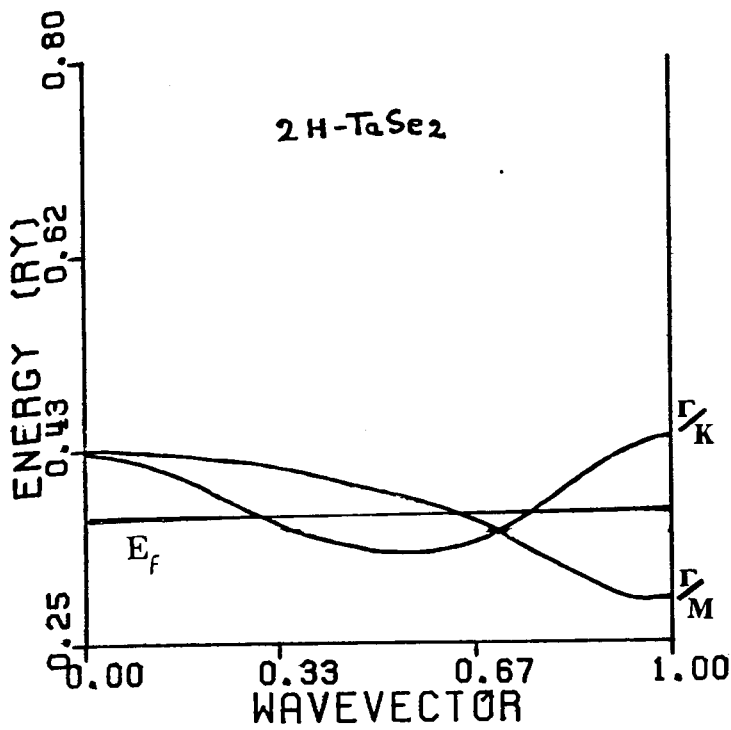


Fig. 1.4a: Energy dependence in  $\Gamma/K$  and  $\Gamma/M$  directions. Note greater width of 1T compared to 2H band. From ref. 6.

Fig 1.4b: Density of states for 1T and 2H TaSe<sub>2</sub>. Note logarithmic 2H behavior against essentially flat 1T behavior.



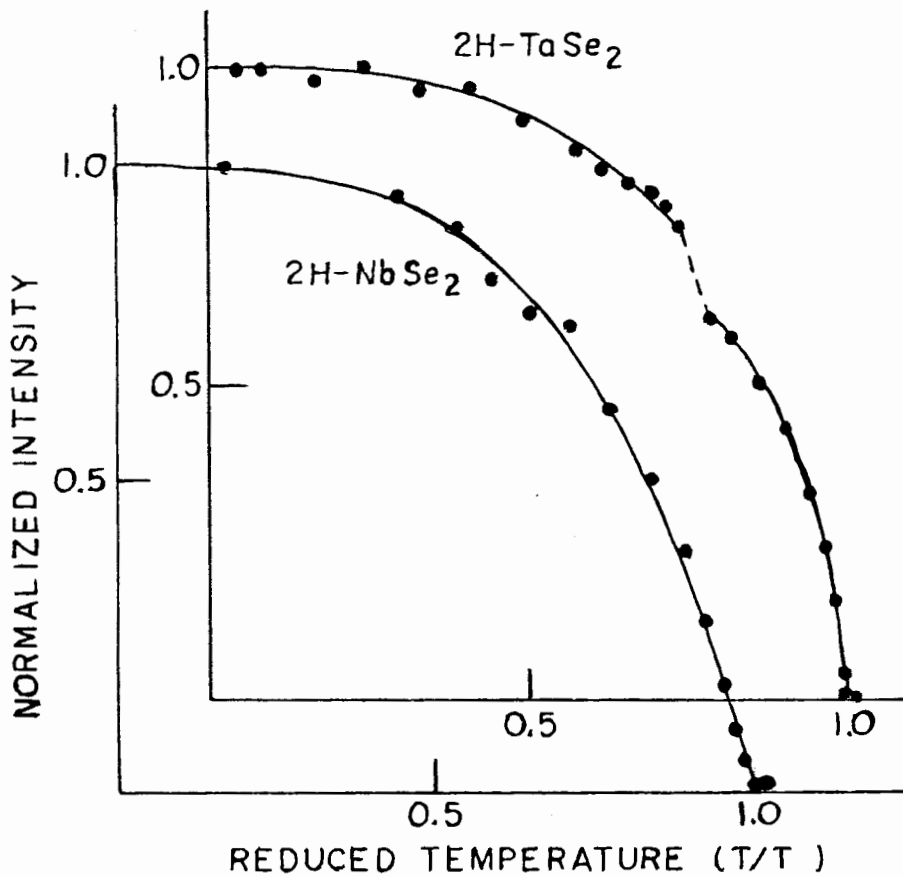


Fig. 1.5: Normalized intensity of the primary superlattice Bragg peaks vs. reduced temperature. The break in the TaSe<sub>2</sub> curve marks the commensurate-incommensurate transition. NbSe<sub>2</sub> is slightly incommensurate for all temperatures below T<sub>c</sub>. (Data from Moncton et al, ref. 13)

CHAPTER 2

FORMULATION OF C.D.W. HAMILTONIAN

2.1 C.D.W. Hamiltonian

Microscopic theories of C.D.W. transitions mediated by electron-phonon coupling<sup>10</sup> usually begin with the Fröhlich Hamiltonian:

$$H = H_{el}^{\circ} + H_{ph}^{\circ} + H_{int} \quad 2-1$$

$H_{el}^{\circ}$  and  $H_{ph}^{\circ}$  describe the eigenvalue spectrum for electrons and phonon respectively in the absence of coupling introduced by  $H_{int}$ :

$$H_{el}^{\circ} = \sum_{\mathbf{k}} \epsilon_{\mathbf{k}}^{\circ} c_{\mathbf{k}}^{\dagger} c_{\mathbf{k}}$$

$$H_{ph}^{\circ} = \sum_{\mathbf{q}} \omega_{\mathbf{q}}^{\circ} b_{\mathbf{q}}^{\dagger} b_{\mathbf{q}} \quad 2-2$$

$$H_{int} = \frac{1}{\sqrt{N}} \sum_{\mathbf{q}} \sum_{\mathbf{k}} I(\mathbf{k}, \mathbf{k} + \mathbf{q} + \vec{G}) c_{\mathbf{k} + \mathbf{q} + \vec{G}}^{\dagger} c_{\mathbf{k}} (b_{\mathbf{q}} + b_{-\mathbf{q}}^{\dagger})$$

where  $\sum_{\mathbf{k}}$  = sum over electronic states of the first Brillouin zone

$\sum_{\mathbf{q}}$  = sum over phonon states of the first Brillouin zone

$\vec{G}$  = reciprocal lattice vector such that  $(\vec{k} + \vec{q} + \vec{G})$  remains

within first Brillouin zone

The  $c_{\mathbf{k}}$ ,  $c_{\mathbf{k}}^{\dagger}$  and  $b_{\mathbf{q}}$ ,  $b_{\mathbf{q}}^{\dagger}$  are the annihilation and creation operators of electrons of momentum  $\vec{k}$  and phonons of momentum  $\vec{q}$  respectively.  $I(\vec{k}, \vec{k} + \vec{q} + \vec{G})$  scatters electrons from  $\vec{k}$  to

$\vec{k} + \vec{q} + \vec{G}$  by either absorbing or emitting a phonon of momentum  $\vec{q}$  or  $-\vec{q}$  and thus destroys the eigenvalue status of  $\epsilon_{\vec{k}}^0$  and  $\omega_{\vec{q}}^0$ . As a problem in many-body field theory, Hamiltonians with this interaction structure, bilinear in the fermion field and linear in the boson field, have been a subject of extensive investigation<sup>14</sup>. Though no exact solution of the full problem exists, solutions consistent with the essential many-body physics can be prescribed.

In the C.D.W. formulation developed by Chan and Heine<sup>10</sup>, as the phase transition is approached from above, dynamic electronic screening originating from  $H_{int}$  and appropriately enhanced by such factors as a nesting Fermi surface, progressively acts to soften a particular phonon mode until at the transition temperature  $T_c$ , the mode in question collapses to zero frequency. In the C.D.W. state, coherent electronic scattering between  $\vec{k}$ ,  $\vec{k} + \vec{q}_0$ ,  $\vec{k} + \vec{q}_0 + \vec{G}$ , etc., where  $\vec{q}_0$  is the wavevector of the soft mode and hence that of the static lattice distortion and  $\vec{G}$  is any reciprocal lattice vector, couples electronic states from above and below the Fermi energy to produce an energy gap at the Fermi surface and a subsequent lowering of the electronic energy.

Within the Chan-Heine model, only a single mode in the phonon Brillouin zone is renormalized by the electron-phonon interaction while a large number of electronic states are coupled by the lattice distortion. Thermodynamic behavior is thus determined by entropy arising from electronic fluctuations across the energy gap with negligible contributions from lattice entropy.

On the other hand, McMillan<sup>11</sup>, proceeding from a Landau free energy expansion in the lattice distortion amplitude rather than an explicit microscopic Hamiltonian, argues that the finite electronic coherence characterized by a length  $\xi_0$  determines an effective width of order  $\Delta k \sim 1/\xi_0$  about  $\vec{q}_0$  in the phonon phase space which is modified by the lattice distortion. In the limit of  $\Delta(T=0)/kT_c \gg 1$ , where  $\Delta(T=0)$  is the zero temperature electronic gap and  $T_c$  is the C.D.W. transition temperature, McMillan<sup>11</sup> neglects electronic entropy entirely and, within a mean field framework, uses only lattice entropy to destabilize the C.D.W. state. In this treatment, the phonons which go soft at  $T_c$  acquire positive frequency below  $T_c$  as vibrations of the order parameter characterizing the lattice distortion.

One aspect of the interacting electron-phonon system not included in the Fröhlich Hamiltonian are anharmonic interactions coupling the normal modes of the lattice. To the extent that phonons, the normal modes of the harmonic Hamiltonian, are well defined, corrections arising from anharmonic contributions are small. For example, in the phonon mediated superconducting transition, the phonon dispersion exhibits no deviation from harmonic behavior, though the electronic spectrum develops a gap at  $T_c$ . However, with the C.D.W. transitions of the 2H layered dichalcogenides, striking modification of the  $\pm G_{1/3}$  L.A.(A) phonons belonging to the star along  $\Gamma$ -M and their surrounding phase space occurs. For

example in  $2H TaSe_2$ , these phonons soften from a high temperature value of  $\approx 8$  meV to  $5$  meV<sup>13</sup> at  $T_C = 120K$ . Below  $T_C$ , the modes derived from the original six equivalent modes experience energy splittings of 2-3 meV about a mean energy of approximately 7.4 meV.

This strong phonon splitting in the C.D.W. state suggests the introduction of anharmonic terms to the Frohlich Hamiltonian as the natural means for describing the Bragg type scattering of the phonon by the static lattice distortion. As a power series expansion of the lattice potential energy  $W(r_1 \dots r_n)$  about its equilibrium value  $W(r_1^0 \dots r_n^0)$ , the anharmonic contribution consists of all terms beyond the quadratic term. Sufficient for our purposes is retention of just the cubic term in this expansion<sup>12</sup>:

$$H_{anh} = \frac{1}{3!} \sum_{i,j,k} \left. \frac{\partial^3 W}{\partial \vec{r}_i \partial \vec{r}_j \partial \vec{r}_k} \right|_0 : \delta \vec{r}_i \delta \vec{r}_j \delta \vec{r}_k \quad 2-3$$

where, as a tensor of the third rank in cartesian coordinate, the symbol  $:$  denotes a triple inner product. Expressing the displacements  $\delta \vec{r}_i$  in terms of the normal mode coordinates  $Q_{q,\lambda}$  of the lattice:

$$\delta \vec{r}_i = \frac{1}{\sqrt{N}} \sum_{q,\lambda} e^{i\vec{q} \cdot \vec{r}_i} \vec{\epsilon}_{q,\lambda} Q_{q,\lambda} \quad 2-4$$

where  $\vec{\epsilon}_{q,\lambda}$  is the polarization vector for the atomic displacements within the unit cell characteristic of the  $\lambda$  mode at wave-

vector  $\vec{q}$ . The condition that the lattice displacement be real requires:

$$Q_{q,\lambda}^* = Q_{-q,\lambda}$$

$$\vec{\xi}_{q,\lambda}^* = \vec{\xi}_{-q,\lambda}$$

2-5

Restricting discussion to a single phonon branch, expression of  $\lambda$  will be subsequently suppressed and the cubic anharmonic contribution can be expressed as:

$$H_{\text{anh}} = \frac{1}{\sqrt{N}} \sum_{q_i, q_j, q_k} V(q_i, q_j) Q_{q_i} Q_{q_j} Q_{q_k} \delta_{q_i + q_j + q_k, G} \quad 2-6$$

$G$  = any reciprocal lattice vector

$$V(q_i, q_j) = \frac{1}{3!} \sum_{\ell, m} \frac{\partial^3 W}{\partial \vec{r}_i \partial \vec{r}_j \partial (\vec{r}_i - \vec{r}_j)} : \vec{\xi}_{q_i} \vec{\xi}_{q_j} \vec{\xi}_{q_k} : e^{i\vec{q}_i \cdot \vec{r}_\ell} e^{i\vec{q}_j \cdot \vec{r}_m}$$

As briefly discussed, motivation for introducing the phonon-phonon scattering generated by the anharmonic interaction is to account for phonon coupling to the static lattice distortion of the C.D.W. state. The lattice distortion itself can be viewed as the acquisition by an appropriate set of normal mode coordinates ( $Q_{q_0}$ ) of a finite expectation value. Physically, this finite expectation  $\langle Q_{q_0} \rangle$  signifies a phase coherence in the atomic displacements from their normal equilibrium position  $r_i^0$ .

For a lattice distortion occurring at wavevector  $\vec{q}_0$  with vector displacement  $\vec{\epsilon}_{\vec{q}_0}$ , the new atomic positions are given by:

$$r_i = r_i^0 + \frac{1}{\sqrt{N}} \sum_q \epsilon_q Q_q e^{iq \cdot r_i} \quad 2-7$$

taking the expectation value:

$$\begin{aligned} \langle r_i \rangle &= r_i^0 + \frac{1}{\sqrt{N}} \left( \epsilon_{q_0} \langle Q_{q_0} \rangle e^{iq_0 \cdot r_i} + \epsilon_{-q_0} \langle Q_{-q_0} \rangle e^{-iq_0 \cdot r_i} \right) \\ &= r_i^0 + \frac{1}{\sqrt{N}} \left( \epsilon_{q_0} \langle Q_{q_0} \rangle + \epsilon_{q_0}^* \langle Q_{q_0}^* \rangle \right) \cos(q_0 \cdot r_i) \end{aligned}$$

since  $\langle Q_q \rangle = 0$  for  $q \neq q_0$

To accommodate this possibility of acquiring a finite expectation value, the normal mode coordinates, as time dependent operators, can be separated into time independent and dependent components:

$$Q_q(t) = \langle Q_q \rangle + \tilde{Q}_q(t) \quad 2-8$$

In the 2H-C.D.W. transition, six independent normal mode coordinates belonging to the star of  $\vec{q}_0$  along  $\Gamma$ -M acquire finite expectation values. Being directly proportional to the lattice displacement, the expectation values of these normal mode coordinates become the appropriate order parameter for the 2H-C.D.W. transitions and are given the form:

$$\langle Q_{q_i} \rangle = 0 \quad T > T_c$$

$$\langle Q_{q_i} \rangle = \sqrt{N} \cdot \Delta \cdot e^{i\theta_{q_i}} \delta_{q_i, q_0} \quad T < T_c \quad 2-9$$

where hexagonal symmetry requires that the amplitude of all expectation values be identical ( $\sim \Delta$ ) and the constraint of real lattice displacement ( $\theta_{q_0} = -\theta_{-q_0}$ ) restricts the number of independent phase factors to 3.

Expressing all lattice degrees of freedom in terms of normal mode coordinates decomposed into static and time dependent components, the model C.D.W. Hamiltonian becomes:

$$H = H_{el}^{\circ} + H_{ph}^{\circ} + H_{int} + H_{anh}$$

$$H_{el}^{\circ} = \sum_K \epsilon_K^{\circ} C_K^{\dagger} C_K \quad 2-10$$

$$H_{ph}^{\circ} = \sum_q \left[ \frac{P_q P_{-q}}{2m_0} + \frac{\lambda_q}{2} (\tilde{Q}_q + \langle Q_q \rangle)(\tilde{Q}_{-q} + \langle Q_{-q} \rangle) \right]$$

$$H_{int} = \sum_q \sum_K I(K, K+q+G) C_{K+q+G}^{\dagger} C_K (\tilde{Q}_q + \langle Q_q \rangle)$$

$$H_{anh} = \frac{1}{\sqrt{N}} \sum_{q_i, q_j, q_k} V(q_i, q_j) (\tilde{Q}_{q_i} + \langle Q_{q_i} \rangle) (\tilde{Q}_{q_j} + \langle Q_{q_j} \rangle)$$

$$(\tilde{Q}_{q_k} + \langle Q_{q_k} \rangle) \delta_{q_i + q_j + q_k, G}$$

where  $(\omega_q^{\circ})^2 = \lambda_0 / m_0$



where  $(\omega_q^0)^2 = \lambda_0/m_0$

From this highly coupled Hamiltonian, the focus of interest will be the mixing of electronic states,  $\epsilon_k^0, \epsilon_{k+q_0}^0, \epsilon_{k+q_0+G}^0 \dots$  etc. as well as normal mode coordinates  $Q_q, Q_{q+q_0}, Q_{q+q_0+G} \dots$  etc. by the static lattice distortion amplitudes [ $\langle Q_{q_0} \rangle$ ]. To this end, the strictly dynamical anharmonic contribution  $\sim Q_{qi} \tilde{Q}_{qj} \tilde{Q}_{qk}$  will be assumed small, as is normally the case, and neglected. The neglect of this purely dynamical anharmonic term restores the model Hamiltonian to harmonic form in the normal mode coordinates except for their coupling to the electrons which essentially renormalize each mode independently. Also, the matrix element for electron-phonon scattering,  $I(k, k+q+G)$ , will be ascribed a constant value equal to  $g$  though, for example, Doran<sup>4</sup> has suggested that the wavevector dependence of this matrix element may be significant in the 2H layered compounds.

With these approximations giving final definition to the model C.D.W. Hamiltonian, solutions to this model are now investigated.

## 2.2 Solutions for Model C.D.W. Hamiltonian

The energy eigenvalues  $\epsilon_k$  and  $\omega_q$  to the model C.D.W. Hamiltonian can be obtained from the equation of motion method for Heisenberg operators:

$$i\hbar \dot{A} = [A, H]$$

2-11

Using the commutation relations

$$C_K^+ C_{K'} + C_{K'} C_K^+ = \delta_{KK'}$$

2-12

$$P_q Q_{q'} - Q_{q'} P_q = \frac{\hbar}{i} \delta_{qq'}$$

and oscillatory solutions of the form:

$$\tilde{Q}_q(t) = e^{i\omega_q t} \tilde{Q}_q$$

2-13

$$C_K(t) = e^{i\epsilon_K t/\hbar} C_K$$

the coupled electron-phonon field equations are simply formulated.

For  $T > T_c$ ,  $\langle Q_{q_0} \rangle = 0$  and the anharmonic term is purely dynamical and, as previously discussed, is neglected. The equations for the field operators in this temperature regime become:

$$-\omega_q^2 \tilde{Q}_q = -\omega_q^0 \tilde{Q}_q + \frac{g}{\sqrt{N} m_0} \sum_K C_{K-q+G}^+ C_K$$

$$\epsilon_K C_K = \epsilon_K^0 C_K + \frac{g}{\sqrt{N}} \sum_q C_{K-q+G} Q_q \quad 2-14$$

As mediator of the Coulomb force, the influence of electronic density fluctuations on phonon frequency renormalization can be drastic, especially at long wavelengths where it is well known that electronic screening reduces the bare longitudinal ionic plasma frequency from a finite value to zero at zero wave-vector.

The equation of motion for the  $C_{k-q}^+ C_k$  coordinate is:

$$i\hbar \overline{C_{k-q}^+ C_k} = \epsilon_k^0 C_{k-q}^+ C_k - \epsilon_{k-q}^0 C_{k-q}^+ C_k + \frac{\delta}{\sqrt{N}} \sum_{q'} [C_{k-q}^+ C_{k-q'} - C_{k-q'+q'}^+ C_k] Q_{q'} \quad 2-16$$

Within the context of the random phase approximation only those states with momentum equal to that of the combined value of the particle and hole are considered. Thus:

$$i\hbar \overline{C_{k-q}^+ C_k} = \epsilon_k^0 C_{k-q}^+ C_k - \epsilon_{k-q}^0 C_{k-q}^+ C_k + \frac{\delta}{\sqrt{N}} (\eta_{k-q} - \eta_k) Q_q$$

$$\text{where } \eta_{k-q} = \langle C_{k-q}^+ C_{k-q} \rangle \quad 2-17$$

In this form, the equation possesses oscillatory solutions:

$$C_{k-q}^+(t) C_k(t) = e^{-i\omega_q t} C_{k-q}^+ C_k$$

$$\therefore C_{k-q}^+ C_k = \frac{\delta}{\sqrt{N}} \frac{\eta_{k-q} - \eta_k}{\hbar\omega_q - \epsilon_k^0 + \epsilon_{k-q}^0} Q_q \quad 2-18$$

Substituting this into the  $Q_q$  equation of motion gives the dynamically screened phonon frequencies:

$$\omega_q^2 = \omega_q^{o2} - \frac{\xi^2}{Nm_0} \sum_K \frac{n_K - n_{K-q}}{\hbar\omega_q - \epsilon_K^o + \epsilon_{K-q}^o} \quad 2-19$$

Beginning with Kohn<sup>12</sup>, it was realized that anomalies in the dynamic electronic susceptibility:

$$\chi(q, \omega) = \sum_K \frac{n_K - n_{K-q}}{\hbar\omega - \epsilon_K + \epsilon_{K-q}} \quad 2-20$$

would be mirrored in the phonon spectrum. Utilizing the concept of nesting Fermi surfaces, first introduced by Lomer<sup>17</sup>, to produce an enhanced electronic susceptibility, Chan and Heine<sup>10</sup> arrive at a criterion for C.D.W. formation in terms of which the softening phonon is driven to zero frequency at the phase transition.

In an alternative model to the usual Fermi nesting scheme, Rice and Scott<sup>9</sup> suggest that saddle points in the two dimensional band structure, located in the vicinity of the Fermi surface, can produce a strongly enhanced susceptibility and in the limit where the Fermi energy and saddle point coincide, a logarithmically diverging susceptibility as  $T \rightarrow 0$ .

On the other hand, while electronic screening significantly renormalizes phonon dispersion, renormalization of electronic energies due to dynamic coupling with the phonons is usually small except for those electrons within the Debye energy of the

Fermi surface. For our purposes it will be assumed that this contribution to the electronic energy can be ignored and, in the same spirit, the dependence of the dynamic susceptibility on phonon frequency  $\omega_q$  will be neglected given that  $\epsilon_k, \epsilon_{k-q} > \omega_q$  for the majority of electronic states.

The equations for the electron and phonon energies thus reduce to

$$\omega_q^2 = \omega_q^{\circ 2} - \frac{\delta^2}{Nm_0} \sum_K \frac{n_K - n_{K-q}}{\epsilon_{K-q}^{\circ} - \epsilon_K^{\circ}} \quad 2-21$$

$$\epsilon_K = \epsilon_K^{\circ}$$

It is worth remarking that the applicability of these assumptions to the 2H layered compounds may not be entirely correct. In the 2H compounds the phonons of interest occur at 8 meV in energy and as it is those electronic states with  $\epsilon_k \approx \epsilon_{k-q}$  which contribute most significantly to the susceptibility, it is not obvious that  $\omega_q$  can be consistently deleted from the denominator of the electronic susceptibility. Also, the problem is compounded by the relative narrowness (1.2 eV) of the conduction band.

We now consider modifications of the equations of motion resulting from a static lattice distortion with Fourier components  $[q_0]$ . The requirement for such a configuration of the system is that it minimizes its total free energy.

The finite values of  $\langle Q_{q_0} \rangle$  are complemented by finite expectation values for the  $[q_0]$  components of the electronic density fluctuation:

$$\langle P_q \rangle = \left\langle \sum_K C_{K+q}^+ C_K \right\rangle \simeq \Delta \cdot \delta \cdot \sqrt{N} e^{i\theta_q} \delta_{q,q_0} \quad 2-22$$

However, since the electronic density fluctuations couple linearly to the lattice coordinates, the static components of the electronic density have no dynamical consequence. The equation of motion for  $Q_q$  and  $C_k$  are:

$$-\omega_q^2 \tilde{Q}_q = -\omega_q^{\circ 2} (\tilde{Q}_q + \langle Q_q \rangle \delta_{q,q_0}) + \frac{\delta}{\sqrt{N}} m_0 \sum_K C_{K-q+G}^+ C_K + \frac{\delta}{\sqrt{N}} \langle P_{-q} \rangle \delta_{-q,q_0} + 3 \sum_{q_i, q_j} [2V(q_i, q_j) \tilde{Q}_{q_i} \langle Q_{q_j} \rangle \delta_{q_j, q_0} + V(q_i, q_j) \langle Q_{q_i} \rangle \langle Q_{q_j} \rangle \delta_{q_i, q_0} \delta_{q_j, q_0}] \delta_{G, q_i + q_j + q_0}$$

$$\epsilon_K C_K = \epsilon_K^{\circ} C_K + \frac{\delta}{\sqrt{N}} \sum_q C_{K-q+G} (\tilde{Q}_q + \langle Q_q \rangle \delta_{q,q_0}) \quad 2-23$$

where again, the dynamical anharmonic contribution  $\sim Q_{q_i} Q_{q_j} Q_{q_k}$  has been neglected.

As noted above, the constant terms in the equation for  $Q_q$  are indicative of the coordinate transformation generated by the lattice distortion but carry no dynamical significance and can be simply transformed away.

Also, as in the case where no static distortion is present, dynamical electron-phonon coupling is neglected in the equation for the electronic coordinate and we have:

$$\begin{aligned}
 -\omega_q^2 Q_q &= -\omega_q^0 Q_q + \frac{g}{\sqrt{N} m_0} \sum_K C_{K-q+G}^+ C_K + 3 \sum_{q_i} \sum_{q_0} V(q q_i) \\
 &\quad Q_{q_i} \langle Q_{q_0} \rangle \delta_{G, q+q_i+q_0} \\
 \epsilon_K C_K &= \epsilon_K^0 C_K + \frac{g}{\sqrt{N}} \sum_{q_0} C_{K-q_0} \langle Q_{q_0} \rangle \quad 2-24
 \end{aligned}$$

As before, the equation of motion applied to  $C_{k-q}^+ C_k$  within the R.P.A. yields the renormalization of  $\omega_q^0$  due to dynamical electronic screening in the presence of the static distortion

$$C_{K-q}^+ C_K = \frac{g}{\sqrt{N}} \frac{n_K - n_{K-q}}{\epsilon_{K-q}(\langle Q_{q_0} \rangle) - \epsilon_K(\langle Q_q \rangle)} Q_q \quad 2-25$$

Thus, within the scope of the approximations employed, electrons and phonon fields, while uncoupled from each other, experience coupling amongst themselves as a result of the static distortion.

Solution to these equations as a proposed description of the C.D.W. phase transition of the 2H layered dichalcogenides will combine a specified set of distortion components  $[q_0]$  with electronic Brillouin zone built from the saddle point model of Rice and Scott<sup>9</sup> and a phonon Brillouin zone inferred from Moncton's<sup>13</sup> neutron results.

The issue of ascribing a set of distortion vectors  $[q_0]$  to the 2H C.D.W. transition is complicated by its incommensurate/commensurate aspect. Citing for 2H TaSe<sub>2</sub><sup>13</sup>:

$$\begin{aligned}
 q_0 &= \pm \frac{G_i}{3} (1-\delta) & \delta \simeq .02 & \quad 120 \text{ K} > T > 95 \text{ K} \\
 q_0 &= \pm G_i/3 & & \quad T < 95 \text{ K} & \quad 2-26
 \end{aligned}$$

The basic observation is that in the incommensurate regime departure from commensurability is a two percent effect and hopefully expressible as a perturbation of the commensurate state. Thus, the distortion amplitudes will be taken as purely commensurate:

$$\langle Q_{q_i} \rangle = \Delta \sqrt{N} e^{i\theta_{q_0}} \quad \begin{matrix} q_0 = \pm G_i/3 \\ T < T_c \end{matrix} \quad 2-27$$

From the work of Holy et al<sup>15</sup>, the Raman activity of the C.D.W. phonon modes implies that they transform as even parity representatives of  $D_{6h}^4$ , the space group of both the C.D.W. and normal phase. This requires that the phases of the distortion amplitudes are all equal:

$$\theta_{q_1} = \theta_{q_2} = \theta_{q_3} = \theta_0 \quad 2-28$$

where  $\theta_0$  is determined by the condition that it minimize the free energy.

### 2.3 C.D.W. Brillouin Zone

#### 2.3A Electronic Zone

With the set  $\{q_0\}$  established at one third of the normal state reciprocal lattice vector, the hexagonal Brillouin zone of the normal state is mapped into a Brillouin zone of again hexagonal symmetry but with one ninth the area. This remapping couples nine distinct  $\vec{k}$ -points of the normal Brillouin zone to one  $\vec{k}$ -point of the reduced zone. Where the distortion energy is small relative to the unperturbed electronic energies, only those  $\vec{k}$ -points with comparable energy will be significantly coupled by the C.D.W. distortion.



The crucial aspect of the electronic Brillouin zone is proposed to be the six equivalent saddle points along  $\Gamma$ -k with explicit positioning of

$$\vec{K}_i = \frac{2}{3} \left( \pm \frac{G_j}{3} \pm \frac{G_K}{3} \right) \quad j \neq K \quad i = 1, 6 \quad 2-29$$

The unperturbed electronic band energy about these six equivalent points is given the simple hyperbolic form:

$$\epsilon_i^0(\vec{K} + \vec{K}_i) = K^2 \cos(2\theta + Ph_i) - \mu \quad 2-30$$

where the chemical potential  $\mu$  locates the Fermi level relative to the  $\vec{K}_i$  Brillouin points and the phase factor  $Ph_i$  runs over six successive sixty degree rotations.

As the logarithmic divergence in the density of states produced by the saddle point regions are assumed to be active element in the C.D.W. transition, these energy profiles are used to generate the entire Brillouin zone. This is consistent with the actual band structure shown in Figure 1.

Due to their assumed location of two-thirds out from  $\Gamma$  along k, scattering from the distortion amplitudes  $\langle Q_{q_0} \rangle$  couples saddle points related by rotations of  $120^\circ$ . The remaining points mapped with the saddle points (see Fig. 3.1) are significantly removed in energy from the saddle points and can be neglected. Thus the energies about the saddle points mix into two separate but equivalent  $3 \times 3$  couplings with the electronic equation of motion expressible as:

$$\epsilon_i C_{\mathbf{k}+\mathbf{k}_i} = \epsilon_i^{\circ} C_{\mathbf{k}+\mathbf{k}_i} + \delta \Delta \left( e^{i\theta_{ij}} C_{\mathbf{k}+\mathbf{k}_j} + e^{i\theta_{ik}} C_{\mathbf{k}+\mathbf{k}_k} \right)$$

where  $\theta_{ij} = -\theta_{ji}$  2-31

The resulting 3 x 3 matrix equation has the form

$$\begin{bmatrix} \epsilon_i^{\circ} - \epsilon & \delta \Delta e^{i\theta_{ij}} & \delta \Delta e^{i\theta_{ik}} \\ \delta \Delta e^{i\theta_{ji}} & \epsilon_j^{\circ} - \epsilon & \delta \Delta e^{i\theta_{jk}} \\ \delta \Delta e^{i\theta_{ki}} & \delta \Delta e^{i\theta_{kj}} & \epsilon_k^{\circ} - \epsilon \end{bmatrix} = 0$$

Where

$$\epsilon_i^{\circ} = K^2 \cos(2\theta)$$

$$\epsilon_j^{\circ} = K^2 \cos(2\theta + 120^{\circ})$$

$$\epsilon_k^{\circ} = K^2 \cos(2\theta + 240^{\circ})$$

2-32

The characteristic equation can be expressed as:

$$\epsilon^3 - \epsilon \left( \frac{3}{4} K^2 + 3(\delta \Delta)^2 \right) - \left( \frac{K^6 \cos 6\theta}{4} + 2(\delta \Delta)^3 \cos \alpha \right) = 0$$

where  $\cos \alpha = \cos(\theta_{ij} + \theta_{jk} + \theta_{ki})$

$$\epsilon_i^{\circ} + \epsilon_j^{\circ} + \epsilon_k^{\circ} = 0$$

2-33

Solution to the resulting cubic equation immediately yields the distortion dependent electronic energies.

$$E_i(k, \theta) = 2 \sqrt{k^4/4 + V^2} \cos[\phi(k, \theta) + P_{hi}]$$

where  $V = \text{electronic gap} = \xi \cdot \Delta$

$$\phi(k, \theta) = \frac{\arccos \left[ \frac{k^6/8 \cos 6\theta + V^3 \cos \alpha}{(k^4/4 + V^2)^{3/2}} \right]}{3}$$

$$P_{hi} = 0^\circ, 120^\circ, 240^\circ \quad 2-34$$

This cubic coupling removes the normal state degeneracy of the saddle points with a splitting of either  $(-2v, +v, +v)$  for  $\cos \alpha = 1$  or  $(+2v, -v, -v)$  for  $\cos \alpha = -1$ . For  $N > 1$ , minimum free energy is achieved with  $\cos \alpha = 1$  while for  $N < 1$ ,  $\cos \alpha = -1$  minimizes the free energy. For  $N = 1$ , given the electron-hole symmetry,  $\cos \alpha = \pm 1$  yields identical free energies.

These energies form the basis for the electronic bands of the reduced C.D.W. zone and will be examined in terms of their Fermi surface topology, optical properties and thermodynamic characteristics in subsequent chapters.

### 2.3B Phonon Brillouin Zone

Focusing upon the phonon coordinates associated with the C.D.W. transition, the neutron work of Moncton et al<sup>13</sup> reveals that the L.A. phonon of A symmetry with  $q_0 = \pm G_{i/3}$  softens as the C.D.W. transition is approached from above. Other phonon branches investigated by Moncton reveal normal dispersion behavior with no suggestion of participation with the developing C.D.W. transition. As the symmetry of the A symmetric L.A. phonons is that of longitudinal displacements of the Ta ions, this corroborates with their coupling to longitudinal electronic fluctuations.

Singling out this A symmetric L.A. phonon and in particular the six equivalent regions about the  $\pm G_{i/3}$  Brillouin points as the C.D.W. active phonon area, the model Hamiltonian offers a coherent picture of the successive stages of phonon renormalization.

As developed earlier, in the normal state the electronically screened phonon frequencies are given by

$$\omega_q^2 = \omega_q^{o2} - \frac{g^2}{NM_0} \rho_{-q} \quad 2-35$$

From Moncton's dispersion results for the A symmetric phonon in  $2HTaSe_2$  at  $T = 300K$  and  $130K$  reproduced in Figure 2.1, the suggestion arises of a screening anomaly in the vicinity of  $q_0 = \pm G_{i/3}$  which is surprisingly insensitive to temperature variation. Interpolating from what would constitute "ideal" L.A.

phonon behavior, a rough estimate hints of an "ideal" 8-9 meV phonon reduced to 7 meV at 300K and 5.5 meV at 130K by electronic screening for wavevector  $q_0 \approx \pm G_{i/3}$ .

With the transition temperature of  $2\text{HTaSe}_2$  at 120K, this calls into question the issue concerning the frequency of the softening mode as the C.D.W. transition is approached from above and the identity they assume in the C.D.W. state. As previously noted, in the Chan and Heine C.D.W. formulation, the phonon mode is driven completely soft at  $T_c$ . Experimentally, Moncton's neutron results substantiate only partial softening as  $T_c$  is approached.

Below  $T_c$ , Lee, Rice and Anderson<sup>19</sup> show that in the incommensurate state invariance of the C.D.W. energy with respect to the translations relative to the underlying lattice implies the existence of a broken symmetry zero frequency mode as  $q \rightarrow 0$  while for a state of commensurability  $M$ , the mode acquires a frequency  $\sim (\Delta/\epsilon_f)^{\frac{M}{2}-1}$  as  $q \rightarrow 0$  where  $\Delta$  is the electronic gap. In passing to the C.D.W. state, modification of the normal modes of interest,  $Q_{q_0}$ ;  $q_0 = \pm G_{i/3}$ , occurs in two basic fashions. First, by renormalizing the electronic energies, the coherent component of  $Q_{q_0}$  alters the electronic susceptibility which dictates the renormalization of  $\omega_{q_0}$ .

Secondly, as new Fourier components of the lattice scattering potential, the coherent amplitudes couple phonons differing in wavevector by  $\Delta \vec{q} = \pm \frac{\vec{G}_i}{3} + \vec{G}_j$  in a Brillouin zone remapping situa-

tion analogous to that described for the electrons. Considering for the moment the  $q_i = \pm G_i/3$  phonons explicitly and neglecting their coupling to the  $\Gamma$  and  $k$  zone points, the equations of motion take the form:

$$\omega_{q_i}^2 \tilde{Q}_{q_i} = \omega_{q_i}^2 \tilde{Q}_{q_i} - \frac{g^2}{Nm_0} \rho_{-q_i} \tilde{Q}_{q_i} + 3\Delta \sum_{j=1}^6 V(q_i, q_j) e^{i\theta_{ij}} \tilde{Q}_{q_j} \quad 2-36$$

The anharmonic potential  $V(q_i, q_j)$  coupling a given vector belonging to the star of six  $G_i/3$  vectors to the other five, has three independent components. Assuming all phase factors to be real,  $V(q_i, q_j)$  is given the parameterized form:

$$V(q_i, q_j) = a \text{ for } q_i + q_j = G/3$$

$$V(q_i, q_j) = b \text{ for } q_i + q_j = G/\sqrt{3} \quad 2.37$$

$$V(q_i, q_j) = c \text{ for } q_i + q_j = \frac{2}{3}G$$

The resulting 6 x 6 matrix equation has the structure:

$$\begin{vmatrix} \omega_q^2 - \omega_q^2 & a & b & c & b & a \\ a & \omega_q^2 - \omega_q^2 & a & b & c & b \\ b & a & \omega_q^2 - \omega_q^2 & a & b & c \\ c & b & a & \omega_q^2 - \omega_q^2 & a & b \\ b & c & b & a & \omega_q^2 - \omega_q^2 & a \\ a & b & c & b & a & \omega_q^2 - \omega_q^2 \end{vmatrix} = 0 \quad 2.38$$

where  $\omega_q^2 \equiv \omega_q^2 - \frac{g^2}{Nm_0} \rho_{-q}(\Delta)$   $q = \pm G_i/3$

Diagonalization of this 6x6 matrix equation yields two nondegenerate and two doubly degenerate eigenfrequencies. Explicit representation of these C.D.W. modes is obtainable from group theory. As representations of  $q=0$  phonons in the reduced zone, the C.D.W. phonons transform as irreducible representations of the  $D_{6h}^4$  space group and are constructed from a coherent superposition of the six  $q=\pm G_i/3$  phonons which transform as representations of A symmetry under  $C_{2v}$ , the maximal symmetry along  $\Gamma-M$ . However, the nonsymmorphic  $D_{6h}^4$  space group can be represented as the product of  $D_{3h}$ , the single layer symmetry, with the inversion operator. When interlayer coupling is weak, as is anticipated here<sup>1</sup>, layer symmetry influences remain strongly embedded in the full crystal symmetry. Neglecting interlayer interactions entirely, the  $q=0$  C.D.W. modes transform as representations of  $D_{3h}$ . Character table analysis readily establishes the representations of the original six A symmetric modes in a C.D.W. state characterized by  $D_{3h}$  symmetry as:

$$\phi_{\text{C.D.W.}} = 2A_1 + 2E' \quad 2-39$$

As  $D_{3h}$  lacks a center of inversion, these four modes are both Raman and infra-red active. In terms of model parameters, the C.D.W. lattice modes have frequencies given by:

Two  $A_1$  modes:

$$\omega_{1,2}^2 = \left( \omega_{G/3}^2 - \frac{\xi^2}{m_0} \rho_{-G/3}(\Delta) \right) \pm \Delta(c + 2a) - 2\Delta b$$

Two E' modes:

$$\begin{aligned}\omega_{3,4}^2 &= \left( \omega_{G/3}^2 - \frac{\xi^2}{m_0} \rho_{-G/3}(\Delta) \right) + \Delta b + \Delta(a-c) \\ \omega_{5,6}^2 &= \left( \omega_{G/3}^2 - \frac{\xi^2}{m_0} \rho_{-G/3}(\Delta) \right) + \Delta b - \Delta(a-c)\end{aligned}\quad 2-41$$

This frequency structure describes the C.D.W. phonons, derived from the  $\pm G/3$  modes and mapped to  $q = 0$  in the reduced zone, as splitting about the frequency:

$$\begin{aligned}\omega_{G/3}^2 - \frac{\xi^2}{m_0} \rho_{-G/3}(\Delta) &\equiv \omega_{\Delta}^2 \\ \text{where } \sum_{i=1}^6 \omega_i^2 &= 6 \omega_{\Delta}^2\end{aligned}\quad 2-42$$

As indicated for the normal phase, the renormalization effected by electronic screening is weakly temperature dependent and to the extent that the saddle point mechanism preserves most of the Fermi surface in the C.D.W. phase,  $\rho_q(\Delta)$  can be anticipated to be not radically different from that of the normal phase.

This is substantiated experimentally. Citing for 2H TaSe<sub>2</sub>, Moncton's neutron work shows a value of 6 meV at 130K just above the phase transition and using the C.D.W. frequencies of Holy et al<sup>15</sup> at 27K yields a value of 7.4 meV for  $(\sum_{i=1}^6 \omega_{q_i}^2)^{1/2}/6$ .

However, to incorporate the influence of gap dependence upon electronic screening,  $\rho_q(\Delta)$  is given the simple parameterization:

$$\rho_q(\Delta) = \rho_q(T_c) + d \cdot \Delta^2 \quad 2-43$$



As developed in Chapter 4, the parameterization of the phonon frequencies utilizes both zero temperature and  $T_c$  phonon frequencies. The task of the theory is to predict the C.D.W. phonon frequencies for  $0 < T < T_c$  from the calculation of  $\Delta(T)$ . Comparison of predicted with experimental C.D.W. phonon frequencies is given in Chapter 5.

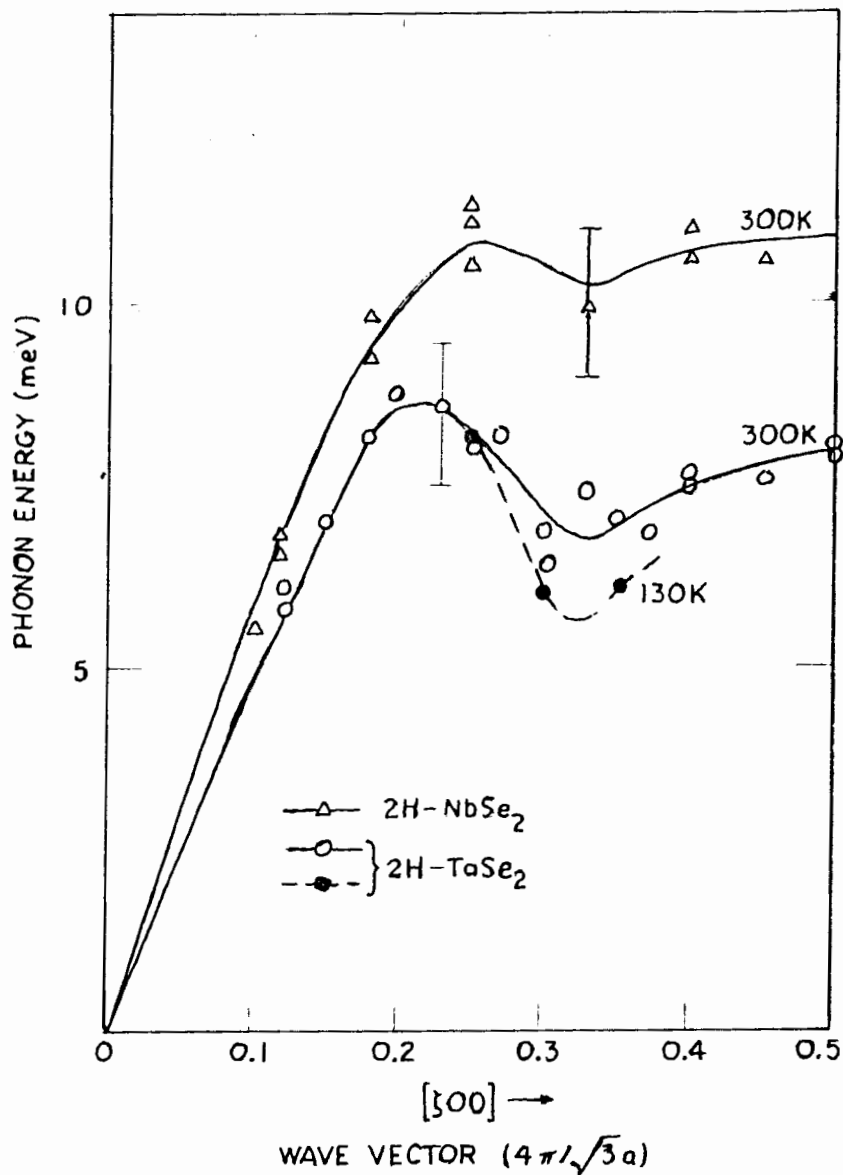


Fig. 2.1: Softening of the L.A.(A) phonon as  $T_c$  is approached from above. Note that between 300K and 130K ( $T_c=120K$ ) the softening is relatively modest. From ref. 13.

3.1 Free Energy Structure

Solutions to the electron-phonon Hamiltonian proposed in the previous chapter, within the terms of reference assumed, separates into dynamical electronic and phonon coordinates and a static component generated by the coherent lattice displacement. Correspondingly, the system's partition function factors into the product of three contributions where the independent thermodynamic variables are the lattice displacement, temperature, volume and chemical potential:

$$Z(\Delta, T, V, \mu) = \text{Tr} e^{-\beta \tilde{H}_{el} - \mu \tilde{N}} \text{Tr} e^{-\beta \tilde{H}_{ph}} \text{Tr} e^{-\beta H_{st}}$$

where  $\tilde{H}_{el} - \mu N = \sum_K (\epsilon_K^\Delta - \mu) C_K^+ C_K$  3-1

$$\tilde{H}_{ph} = \sum_q \hbar \omega_q(\Delta) b_q^+ b_q$$

$$H_{st} = 6 \cdot \frac{1}{2} m_o \omega_{q_o}^2 \Delta^2 + \Delta^3 \left( \sum_{i,j} V(q_i, q_j) \right)$$

As particle number is not conserved for phonons, the associated chemical potential is zero, leaving a single chemical potential  $\mu$  to ensure electron conservation. Also, as the displacement amplitude occurs with finite wavevector the C.D.W. transition conserves volume and its inclusion is unnecessary and it will be omitted.

Given the partition function, the thermodynamics of the electron-phonon system directly follows from the Helmholtz free energy:

$$F(\Delta, T, N) = F_{el}(\Delta, T, N) + F_{ph}(\Delta, T) + F_{st}(\Delta)$$

$$F_{el}(\Delta, T, N) = \mu N - kT \sum_{\mathbf{k}} \log(1 + e^{-\beta(\epsilon_{\mathbf{k}} - \mu)})$$

$$F_{ph}(\Delta, T) = kT \sum_{\mathbf{q}} \log(1 - e^{-\beta \hbar \omega_{\mathbf{q}}}) \quad 3-2$$

$$F_{st}(\Delta) = \mathcal{H}_{st}$$

As it is the phonons about  $g = \pm G_{i/3}$  which are significantly influenced by the distortion, other portions of the phonon Brillouin zone are insensitive to the distortion and can be neglected. Neglecting dispersion in the vicinity of  $\pm G_{i/3}$ , a reasonable assumption for L.A. phonons removed from the zone center, the sum over phonon coordinates is then approximated by an effective weight  $W_0$  which characterizes the phase space area about  $\pm G_{i/3}$  affected by the lattice distortion. For the two dimensional model assumed here,  $W_0$  is the product of the widths of the Kohn anomalies about  $G_{i/3}$  in the  $\Gamma$ -M and  $\Gamma$ -K directions. The form of the Kohn anomaly is determined experimentally by neutron scattering experiments.

Moncton's neutron<sup>13</sup> work indicates a relatively extensive width of  $\sim G/6$  in the  $\Gamma$ -M direction while the width in the  $\Gamma$ -K direction was not determined. Assuming a  $\Gamma$ -K width of  $\Delta q \sim G/8$ ,

relative to a maximum weight of one for the entire zone area,  $W_0$  is of the order of  $\sim 0.1$ . The phonon Brillouin zone is thus distilled to the six C.D.W. coupled  $\pm G_{i/3}$  phonons weighted by the factor  $W_0$ .

The band structure calculations of Mattheiss<sup>6</sup> and Wexler and Woolley<sup>8</sup> furnish the starting point for discussion of the electronic Brillouin zone. As layer-layer interactions are neglected in the model Hamiltonian, the two conduction bands, which arise because of the two layer units per unit cell in the 2H structure, are degenerate and two dimensional. Figures 1.3 and 1.4 display the major features of the conduction bands. These are maxima at  $\Gamma$  and  $k$ , a minimum close to but not exactly at M and saddle points along  $\Gamma$ - $k$ .

The positions of the  $\Gamma$ - $k$  saddle points, both in  $\vec{k}$  space along  $\Gamma$ - $k$  and in energy relative to the Fermi energy, are not well established. Mattheiss gives a saddle point location of  $\frac{2}{3}$   $\Gamma$ - $k$  set slightly below the Fermi surface while Wexler and Woolley find a location a approximately  $\frac{1}{2}$   $\Gamma$ - $k$  and displaced  $\sim 0.2$  meV below the Fermi surface.

For the  $\Gamma$ - $k$  saddle points to effectively couple to the  $G_{i/3}$  C.D.W. distortion, the  $\frac{2}{3}$   $\Gamma$ - $k$  position (one third would also suffice) is needed and this value will be assumed.

Density of state calculations in the 2H layered compounds as performed by Mattheiss and later by Doran et al<sup>4</sup> for  $NbSe_2$ , indicate a large peak at midband, slightly below the Fermi

energy, which drops off to either band edge. This peaked structure we attribute to the saddle point regions where the density of states acquires a logarithmic dependence while the remaining portions of the zone are assumed to contribute an essentially constant background component characteristic of two dimensional behavior.

Focussing our attention on the saddle point regions as the active electronic agent in the C.D.W. transition, hyperbolic energy surfaces are used to parameterize dispersion about the six saddle points. Assuming electron-hole symmetry we have:

$$\xi_i(\vec{k}) = K^2 \cos(2\theta + \text{Ph}_i) \quad \text{Ph}_i = n\pi/3 \quad n=1,6 \quad 3-3$$

where the phase  $\text{Ph}_i$  gives the relative orientation of the saddle points to some fixed  $k$  direction.

Though a reasonable facsimile of the energy dispersion for roughly two-thirds the zone, it obviously falters in the  $\Gamma$  and  $K$  regions as well as along the  $\Gamma$ - $M$  lines where the energy surfaces intersect abruptly, rather than continuously. However, cognizant of these limitations, the proposal that the essential thermodynamics of the C.D.W. phase transition is generated by states about the saddle point region suggest that the hyperbolic energy parameterization is a reasonable characterization of the relevant electronic band features.

With the saddle point energy below the Fermi energy, Figure 3.1 illustrates the mapping of the parent hexagonal zone into the nine reduced zones of reciprocal lattice vectors  $G_{i/3}$ . The Fermi surfaces portrayed are those, except for the perpendicular intersection at zone boundaries, which characterize the normal state. The Fermi surface of zones 2, 3 and most of 4 and 8 are expected to be essentially unaffected by the C.D.W. distortion.

As the saddle points are the focus of attention, with the introduction of  $G_{i/3}$  coupling a model which extracts the 3 x 3 saddle point coupling from the full 9 x 9 matrix is employed to describe influences of the C.D.W. upon the electronic energy band. The Brillouin zone is thus approximated by circular areas of radius  $k_0$  about the saddle points such that the combined areas equal that of the full hexagonal zone:

$$6\pi k_0^2 = G^2 \sqrt{3}/2$$

$$k_0 = 0.23 G$$

3-4

The electronic energy within the  $k_0$  circular regions is obtained by extrapolating solutions from the cubically coupled (3 x 3) energy sheets. By superimposing the energies of the three saddle points as they are coupled by the  $G_{i/3}$  C.D.W. distortion, Figure 3.2 shows both the actual Brillouin zone, using the reference scheme of Figure 3.1, and the model device of an

area inscribed by  $k_0$  radius. It is evident that  $k_0$  area procedure fails to include the hexagonal zone geometry and over-extends the validity of the  $3 \times 3$  factorization from the full  $9 \times 9$  coupling matrix.

However, except where detailed C.D.W. Fermi surface features are to be inferred as discussed later, the representation formed from the cubically coupled hyperbolic energy sheets situated symmetrically about two-thirds  $\Gamma$ -K can be expected to properly analyze that feature correlated with the C.D.W. state, the midband peak in the density of states.

Thus, for the purpose of calculation, the sum over the two dimensional electronic band is replaced by integration about the six circular areas.

Using symmetry to reduce angular integrations to a  $\pi/6$  interval, introducing the variable substitution  $k' = k^2/2$ , replacing  $k_0^2$  by an effective electronic bandwidth  $\omega_c$  and including a factor of two for spin, the Brillouin zone sum has the normalized form:

$$\sum_{\mathbf{k}} = \frac{4}{\pi \omega_c} \sum_{i=1}^3 \int_0^{\pi/6} d\theta \int_0^{\omega_c/2} dk = 2 \quad 3-5$$

As the  $G_{i/3}$  distortion couples the six saddle points into equivalent  $3 \times 3$  couplings, the sum over six saddle points is condensed into a sum over three regions.

Having isolated and characterized the features of the electron and phonon Brillouin zone deemed responsible for the



C.D.W. phase transition, the total free energy is given the explicit form:

$$F_{el}(\Delta, T, N) = \mu N - kT \frac{4}{\pi \omega_c} \sum_{i=1}^3 \int_0^{\pi/6} d\theta \int_0^{\omega_c/2} dk \log \left( 1 + e^{\beta(E_i - \mu)} \right)$$

$$F_{ph}(\Delta, T) = kT W_0 \sum_{i=1}^6 \log \left( 1 - e^{-\beta \hbar \omega_{q_i}(\Delta)} \right) \quad 3-6$$

$$F_{static}(\Delta) = 6 \cdot \frac{1}{2} m_0 \omega_0^2 \Delta^2 + \Delta^3 \left( \sum_{i,j} V(q_i, q_j) \right)$$

Requiring that the free energy be stationary with respect to  $\Delta$  and an absolute minimum relative to the  $\Delta = 0$  solution establishes the criterion for a finite lattice distortion. Deferring for the moment explicit numerical solution to these equations with a parameterization appropriate to the 2H layered dichalcogenides, a short discussion of the rich thermodynamics contained in these free energy expressions will be given.

### 3.2 Saddle Point Model

At  $T = 0$ , the phonon contribution to the total free energy vanishes as the ground state of any lattice contains no dynamical excitations (phonons), leaving only electronic and static contributions to establish the distortion magnitude. This ignores the zero point energy of the phonon which is reduced by at least an order of magnitude by the phase space constraint ( $W_0 \leq .1$ ) from the static distortion energy.

In models based on a nesting Fermi surface mechanism, the electronic free energy contains a negative logarithmic contribution  $\sim \Delta^2 \log(\Delta/\omega_c)$  which is always sufficient to energetically override the quadratic lattice strain energy and guarantees a finite distortion at  $T = 0$

The zero temperature distortion and the ensuing thermodynamics, where phonon entropy can be ignored, mathematically parallels the energy gap equation of B.C.S. theory in the weak coupling limit. The resulting energy gap solutions usually employ the assumption that variations in the density of states over a range set by the energy gap are small and can be neglected.

The saddle point mechanism, on the other hand, features a logarithmic density of state structure in the vicinity of the Fermi energy. Density of state variations on a scale of the energy gap can be significant and the approximation of a constant density of states is no longer applicable. By the same argument, variations in the chemical potential induced by the energy gap must be accounted for to ensure particle number conservation.

As in the B.C.S. theory, a perfectly nesting fermi surface produces a zero temperature energy gap related to the transition temperature by:

$$2\Delta(0) = 3.5 kT_c \quad (3-7)$$

The Debye frequency cutoff of the B.C.S theory is replaced by the electronic bandwidth  $\omega_c$ . The saddle point formulation couples the logarithmic Van Hove singular points of the electronic Brillouin zone. As such it is not directly pinned to the Fermi surface though it will only be effective if the saddle points are nearby to the Fermi level and are modified by the C.D.W. distortion.

The existence of an energy separation between the saddle point singularity and Fermi energy destroys the characteristic B.C.S. logarithmic gap dependence in the electronic free energy as integrals of the form:  $\lambda = \int_0^{\omega_c} dk / \sqrt{k^2 + \Delta^2}$  are supplanted by  $\lambda = \int_{\mu}^{\omega_c} dk / \sqrt{k^2 + \Delta^2}$ . Thus, non zero solutions to the zero temperature gap equation are not necessarily assured. The position of the Fermi energy relative to the saddle point assumes a pivotal role.

### 3.3 Phonon Free Energy

At finite temperature, phonon excitations make a contribution to the total free energy. The influence of phonon entropy upon the stability of the C.D.W. phase depends upon the modifications lattice distortion introduces into the phonon frequency spectrum and the extension of these modifications into the Brillouin zone.

Within the context of the model Hamiltonian, frequency modifications are of two types. First, there are "self energy"

effects which modify all frequencies by equivalent amounts and second, anharmonic coupling which splits the frequency degeneracy about the self energy corrected frequency value.

If frequency splitting is neglected, the phonon free energy, relative to the zero distortion state, will increase for positive self energy contributions and decrease for negative self energy contributions. If, on the other hand, self energy corrections associated with lattice distortion are neglected, anharmonic splitting always produces a lowering of the phonon free energy relative to the unsplit configuration.

In the 2H layered dichalcogenides the proposal is that the positive self energy corrections combined with significant anharmonic splitting cancel to a large degree. The positive self energy reflects the reduced effectiveness of electronic screening at the distortion wavevector in the distorted state. However, dramatic alterations of the electronic response between C.D.W. and normal state are not anticipated as the saddle point model involves only a small portion of the Fermi surface. Experimentally, this is reasonable since the drop in the magnetic susceptibility between  $T_c$  and zero degrees is only  $\sim 25\%$ .

In the event that splitting dominates self energy effects, lattice entropy is higher in the distorted configuration, due to occupancy of those modes split to lower energy, and thus acts to promote rather than destabilize the C.D.W. phase. However, given that the mean C.D.W. phonon frequency at zero

degree is 7.4 meV compared with a phonon energy of 5 meV at  $T_c$  for 2H TaSe<sub>2</sub>, numerical results of the next chapter attribute to the phonons a destabilizing influence on the C.D.W. state, as developed by McMillan<sup>11</sup>.

While the possibility arises for the phonons in the C.D.W. state to have greater entropy and thus lower free energy than the phonons of the zero distortion state, the electronic entropy can only serve to destabilize the C.D.W. structure as thermal smearing of the Fermi surface annuls the distinction between C.D.W. and normal configuration.

The nesting Fermi surface model as used by Chan and Heine involves only a single phonon mode thus  $W_0$ , as measure of participating phonon phase space, is essentially zero. However, citing for 2H TaSe<sub>2</sub> where  $T_c = 120K$  and infrared work of Barker et al<sup>20</sup> indicates new features in the optical absorption below 120K at  $\sim .25$  meV, McMillan suggests the inapplicability of electronically driven B.C.S. scaling to the 2H C.D.W. transition since:  $\Delta(0) \approx 20 kT_c$ .

Proposing a reformulation based on a correlation length  $\xi_0$  which defines the distance scale over which the electronic gap (wavefunction) is coherent, the premise is that, as the electrons can not distinguish phonons differing by  $\Delta q \sim 1/\xi_0$ , phonons within  $\Delta q \sim 1/\xi_0$  of the distortion wavevector are renormalized.

These  $\Delta q < 1/\xi_0$  C.D.W. phonons, having been driven soft at  $T_c$ , are reinstated to finite frequency below  $T_c$  purely as vibrations of the C.D.W. distortion amplitude and thus constitute a higher free energy state than the zero frequency condition.

In the limit that  $\Delta(0)/kT_c \gg 1$ , McMillan<sup>11</sup> argues that mounting phonon entropy drives the C.D.W. transition as the large  $\Delta(0)/kT_c$  ratio suppresses electron excitations across the gap..

As numerical work in the next chapter suggest, McMillan's phonon entropy mechanism appears operative to some degree in the 2H system.

As previously emphasized, the experimentally realized condition for the 2H layer compounds of a substantially finite phonon frequency ( $\sim 5$  meV) at  $T_c$  with splitting below  $T_c$  coupled with band structure calculations (Mattheiss) indicating perhaps greater saddle point than nesting character supports the re-normalization mechanism features through the model Hamiltonian. No correlation length  $\xi_0$  appears to implicate phonons as they couple directly to the lattice distortion. In the next chapter, the thermodynamics of the model Hamiltonian is quantitatively developed.

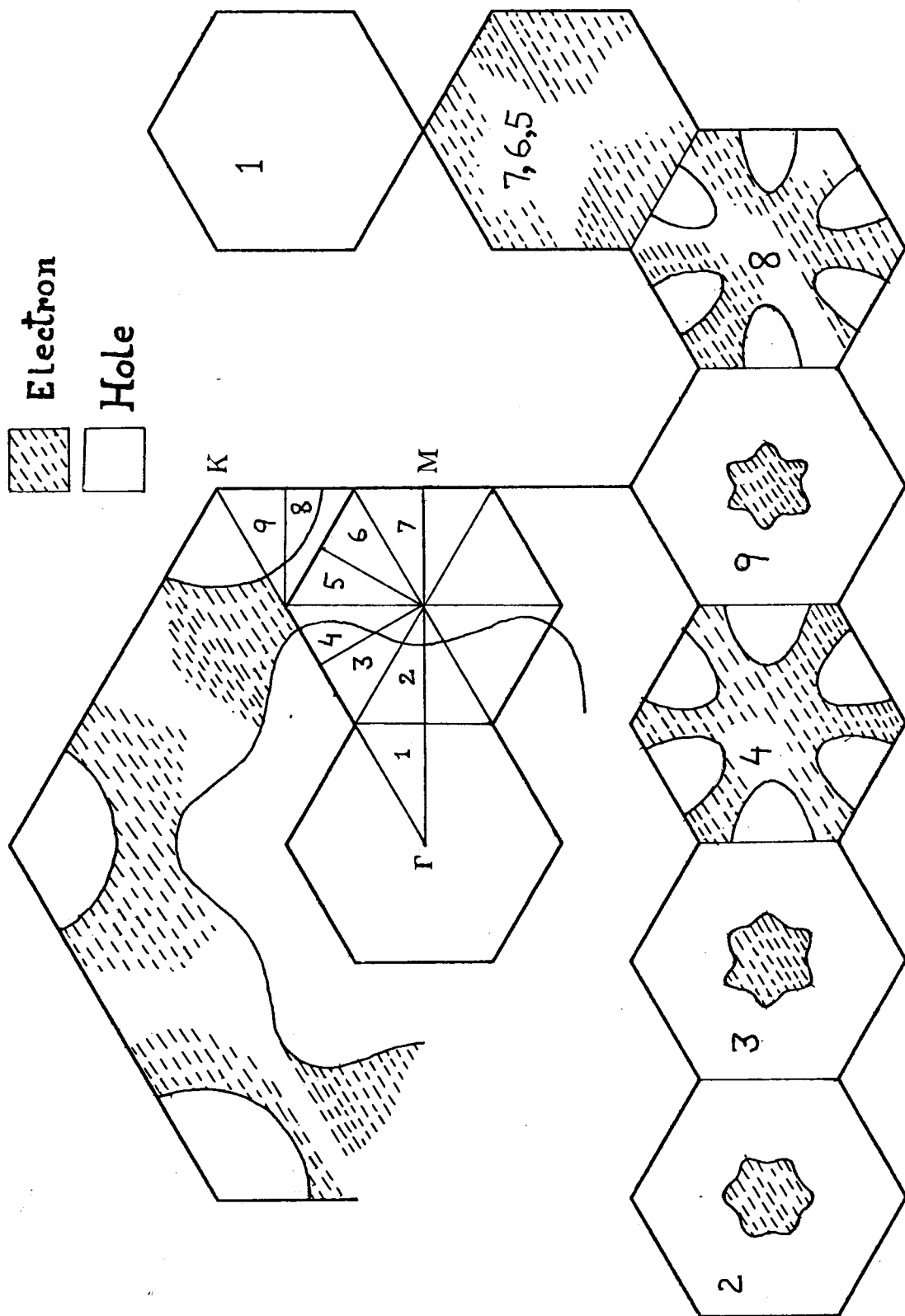


Fig. 3.1:  $\bar{G}/3$  remapping of normal state full zone assuming no electronic alteration except perpendicular intersection of zone boundary. Illustrated Fermi surfaces are qualitative. Compare with Fig. 5.1

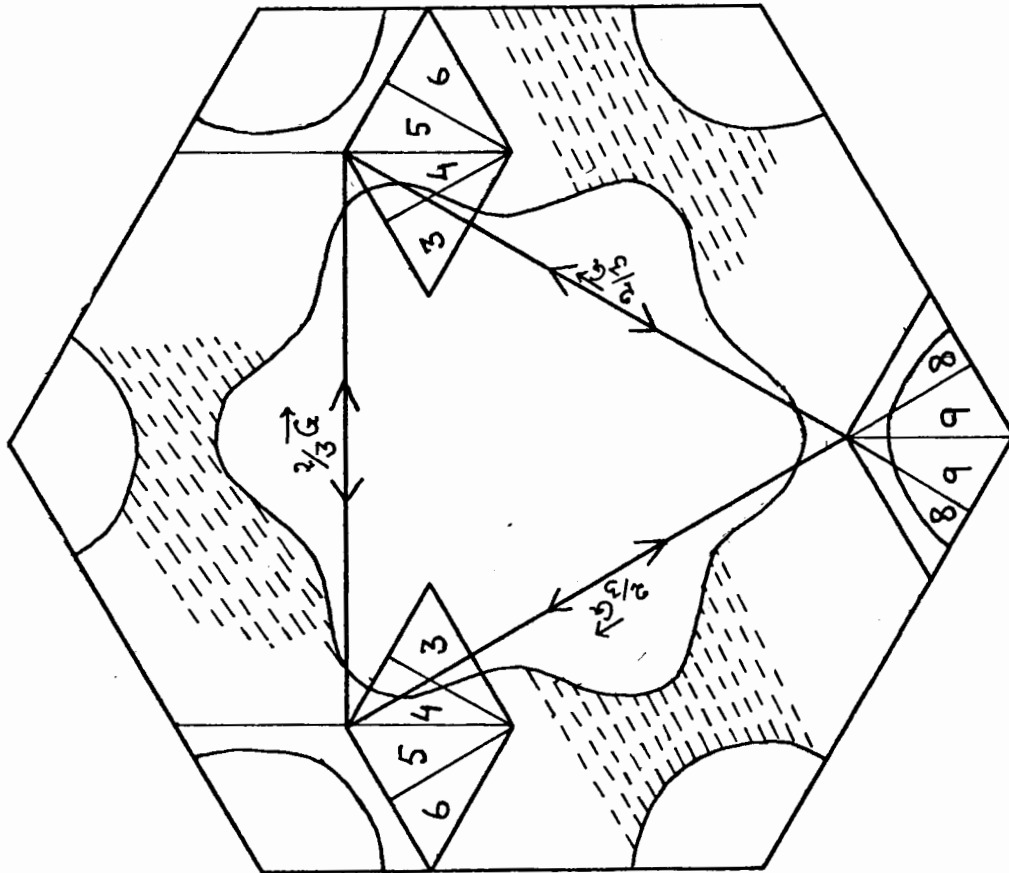


Fig. 3.2a: location of band sections from the parent zone coupled by the  $\frac{2}{3}\vec{G}$  C.D.W. distortion.

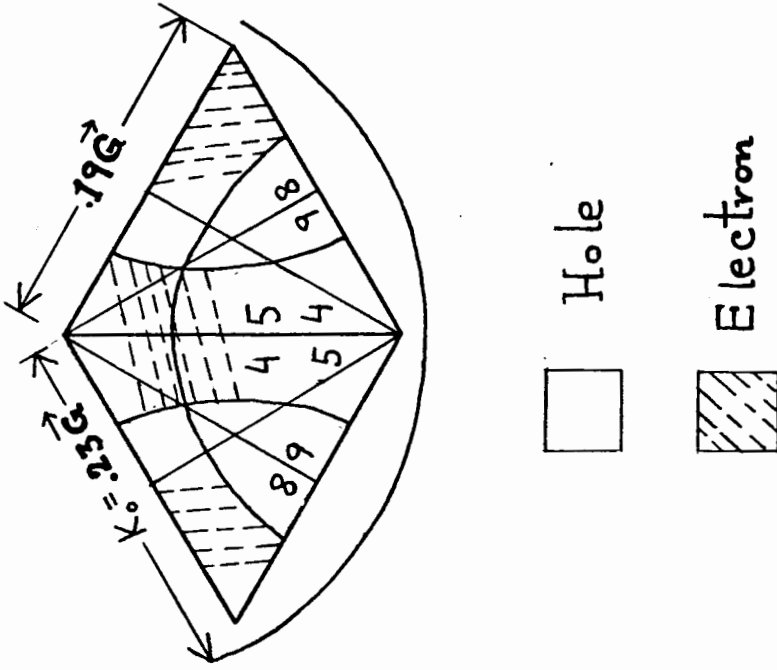


Fig. 3.2b: Superposition of energy sections (4,5,8) and (4,5,9) which couple in the saddle point model. Also shown is the effective radius  $K_0$  radius relative to actual Brillouin scale.



CHAPTER 4

NUMERICAL RESULTS OF SADDLE POINT MODEL

4.1 Parameters of C.D.W. State

Summarizing the results of the last two chapters, the total free energy per unit cell of the electron/lattice system reduces to the sum of electronic, phonon, and static contributions.

$$F(N, T, \Delta) = F_{el}(N, T, \Delta) + F_{st}(\Delta) + F_{ph}(T, \Delta) \quad 4-1$$

The electronic contribution consists of two dimensional integrals over circular Brillouin zone sections centered on the  $\Gamma$ -K saddle points:

$$F_{el}(N, T, \Delta) = -\frac{KT \cdot 8}{\pi \omega_c} \sum_{i=1}^3 \int_0^{\pi/6} d\theta \int_0^{\omega_c/2} dk \log \left( 1 + e^{-\beta(E_i - k)} \right) \quad 4-2$$

$\omega_c$  = electronic band width

$$E_i(K, \theta) = 2 \sqrt{K^2/4 + V^2} \cos \left[ \frac{\arccos \left( \frac{K^3 \cos 6\theta + V^3 \cos \alpha}{[K^2/4 + V^2]^{3/2} + Ph_i} \right)}{3} \right]$$

$V$  = electronic gap =  $\xi \cdot \Delta$

$Ph_i = 0^\circ, 120^\circ, 240^\circ$

$\cos \alpha = \text{C.D.W. lattice phase} = \begin{matrix} +1 & N > 1 \\ -1 & N < 1 \end{matrix}$

The static component depends only upon the C.D.W. distortion amplitude  $\Delta$ :

$$F_{st}(\Delta) = \frac{1}{2} 6 m_0 \omega_G^0 \Delta^2 + \Delta^3 \left( \sum_{i,j} V(q_i, q_j) \right) \quad 4-3$$

The phonon component is described by the free energy of the six  $q_0 = \pm G_{i/3}$  L.A. (A) phonons weighted by  $W_0$ :

$$F(\Delta, T) = W_0 kT \sum_{i=1}^6 \log \left( 1 - e^{-\beta \hbar \omega_{q_i}} \right) \quad 4-4$$

$$W_0 \leq 1$$

$$A_1 \xi \text{ modes: } \omega_{1,2}^2 = \left( \omega_{G/3}^2 - \frac{\xi^2}{m_0} \rho_{-G/3}(T_c) + d\Delta^2 \right) \pm \Delta(c+2a) - 2\Delta b$$

$$E_2 \xi \text{ modes: } \omega_{3,4}^2 = \left( \omega_{G/3}^2 - \frac{\xi^2}{m_0} \rho_{-G/3}(T_c) + d\Delta^2 \right) + \Delta b + \Delta(a-c)$$

$$E_2 \xi \text{ modes: } \omega_{5,6}^2 = \left( \omega_{G/3}^2 - \frac{\xi^2}{m_0} \rho_{-G/3}(T_c) + d\Delta^2 \right) + \Delta b - \Delta(a-c)$$

The properties of this free energy structure depends sensitively upon the parameter set employed. The electronic energy scale is established by the conduction bandwidth  $\omega_c$ , typically  $\sim .6$  eV using 2H TaSe<sub>2</sub> as the paradigm of the 2H layered compounds while the relevant phonon energy,  $\omega_q$ , together with an effective mass  $m_0$ , typically 7 meV and 200 A.M.U. respectively, determine the lattice distortion energy scale.

In addition, the electronic concentration  $N$ , though properly equal to unity as one electron per unit cell is contributed to the conduction band, will be given parameter status to compensate for incompleteness in the model band structure. As model calculations proceed from symmetric hyperbolic energy surfaces centered at the  $\Gamma$ -K saddle points, the  $N = 1$  condition rather artificially places the Fermi energy exactly at the saddle point energy. To simulate displacement of the saddle point below the Fermi energy, as indicated by band structure calculations, a range of electronic concentrations are considered. Explicitly,  $N = 1, 1.1, 1.2$  and  $1.3$  are investigated.

The essential parameter of the theory, the electron-phonon coupling  $g$ , linearly relates the electronic energy gap to the static lattice distortion and thus correlates electronic and lattice energy scales. To establish the magnitude of this crucial parameter, contact is made with the temperature dependence of the  $q = G_{i/3}$  L.A. phonon for  $T > T_c$ . As previously discussed, the phonon frequencies are renormalized by the dynamic electronic susceptibility

$$\omega_q^2(T) = \omega_q^2 - \frac{\delta^2}{m_0} \chi_q(T)$$

$$\chi_q(T) = \sum_K \frac{\eta(\epsilon_K) - \eta(\epsilon_{K+q})}{\epsilon_{K+q} - \epsilon_K} \quad 4-5$$

Momentarily deferring discussion of explicit numerical techniques, Fig. 4.1 displays the  $g = \pm G_{i/3}$  (equivalent to  $\pm 2/3 G_i$ ) electronic susceptibility as a function of temperature where for  $N = 1$  at zero temperature the susceptibility diverges logarithmically. While the saddle point model can be expected to satisfactorily characterize the degree of variation in electronic quantities, which are postulated to arise primarily from the  $\Gamma$ -K saddle point regions, estimates of absolute quantities, which reflect more the global properties of the band structure, are less reliable.

From Moncton's<sup>13</sup> neutron work, revealing the  $q = G_{i/3}$  L.A. phonon softening from an energy of 7 meV at 300K to 5.5 meV at

130K in conjunction with the susceptibility change predicted by the saddle point model over this temperature range, the electron-phonon coupling constant can be deduced as follows.

Decomposing the electronic susceptibility into temperature independent and dependent components, the renormalized phonon frequency can be expressed as:

$$\omega_q^2(\tau) = \omega_q^{\circ 2} - g^2/m_0 (\chi_q^{\circ} + \chi_q'(\tau)) \quad 4-6$$

$$\text{where : } \chi_q(\tau) = \chi_q^{\circ} + \chi_q'(\tau)$$

As the eigenvalue of the harmonic Hamiltonian,  $\omega_q^{\circ}$  can be consistently redefined to include the constant renormalization factor of  $\frac{g^2}{m_0} \cdot \chi_q^{\circ}$  while from Fig. 4.1 it is sufficient to measure  $\chi_q^1(\tau)$  relative to its 600K value as variations beyond this temperature are small and can be neglected. The quantities  $\omega_q^{\circ}$  and  $g^2/m_0$  are now established by the conjunction of experimental data with susceptibility variation from the following relations

$$\omega_q^2(300K) = \omega_q^{\circ 2} - g^2/m_0 (\chi(300K) - \chi(600K)) \quad 4-7$$

$$\omega_q^2(130K) = \omega_q^{\circ 2} - g^2/m_0 (\chi(300K) - \chi(600K))$$

where  $\hbar\omega_q(300K) = 7 \text{ meV}$

$\hbar\omega_q(130K) = 5.5 \text{ meV}$

Using Fig. 4.1, where the susceptibility is in units of  $\omega_c^{-1}$ , to establish the relevant  $\chi(T)$  values, we have:

	$\hbar\omega_q^0$	$\hbar^2 g^2 / m_0$ (units of $\text{meV}^2 \cdot \omega_c$ )
N = 1.	8.1 meV	71.4
= 1.1	8 meV	117.6
= 1.2	8.6 meV	375.

4-8

For N greater than 1.2, the effect of the logarithmic density of states singularity upon the temperature dependence of the susceptibility is annulled by depression below the Fermi energy.

The values for  $\omega_q^0$  are in line with values obtained by extrapolating out electronic influences from the  $q = G_i/3$  L.A. phonon.

More relevant, however, is the combination  $\omega_q^{0^2} m_0 / g^2$  and the magnitude of g itself.

To accentuate only those parameters essential to the saddle point model, only the quadratic term of the static free energy contribution is retained for subsequent calculations. The distortion energy of the lattice in the C.D.W. state then involves only the combination  $\omega_q^{0^2} m_0 / g^2$  and assumes the form:

$$F_{st}(\Delta) = \frac{1}{2} \cdot 6 \cdot m_0 \omega_q^{0^2} \Delta^2 = \frac{1}{2} \cdot 6 \cdot \frac{m_0 \omega_q^{0^2}}{\delta^2} V^2 = \frac{1}{2} \delta' V^2 \quad 4-9$$

where  $g'$  measures the effective lattice stiffness. Using the compiled results for  $\omega_q^0$  and  $g^2/m_0$  and measuring all energy quantities in units of the bandwidth  $\omega_c$ ,  $g'$ , in units of  $\omega_c^{-2}$ , assumes the values:

$$\begin{aligned} g' &= 5.46 & \text{for } N = 1 \\ &3.2 & \text{for } N = 1.1 \\ &1.2 & \text{for } N = 1.2 \end{aligned} \tag{4-10}$$

Preempting results from the numerical calculations which employ  $g'$  in the range 2-3, the zero temperature electronic energy gap is of the order  $v \approx .15 \omega_c$ . Using this together with values of  $\omega_c = .6$  eV for the bandwidth and  $m_0 = 200$  A.M.U. for the effective mass,  $g$  and hence the static distortion of the lattice can be determined. The results, for  $v = .15 \omega_c$ , are:

$$\begin{aligned} g &= 1.43 \text{ eV/\AA} & \text{for } N = 1 \\ &1.83 \text{ eV/\AA} & \text{for } N = 1.1 \\ &3.37 \text{ eV/\AA} & \text{for } N = 1.2 \end{aligned} \tag{4-11}$$

$$\begin{aligned} \therefore \Delta &= .06 \text{ \AA} & \text{for } N = 1 \\ &.05 \text{ \AA} & \text{for } N = 1.1 \\ &.027 \text{ \AA} & \text{for } N = 1.2 \end{aligned}$$

Experimentally, Moncton<sup>13</sup> determined  $\Delta$  for 2H TaSe<sub>2</sub> to be between .05 and .09 angstroms. These experimental results compare quite favorably with those anticipated by the saddle point model from a coupling constant extracted purely from phonon and electronic susceptibility behaviour for  $T > T_c$ .

Turning to the phonon contribution to the free energy, it is expressible in terms of the phonon frequency spectrum together with  $W_0$ , the extent of participating phonon Brillouin zone. As previously discussed, the width of the Kohn anomaly suggests that  $W_0 \approx .1$ . To contrast the purely electronically driven transition,  $W_0 = 0$ , with the mixed electron and phonon free energy situation, numerical calculations will examine both the  $W_0 = 0$  and  $W_0 = .1$  case.

The phonon frequency spectrum at  $T = 0$  and  $T = T_c$  will be taken from established experimental results. This suffices to establish the unknown constants characterizing to the two  $A_{1g}$  and two  $E_{2g}$  modes. Already the phonon energy at 130K and 300K have been explicitly used to establish the electron-phonon coupling constant. It will be the object of the theory to predict the temperature dependence of the phonon energy between zero degrees and  $T_c$  as well as for  $T > T_c$ .

#### 4.2 Method of Calculation

As elaborated in the previous section, the parameters pertinent to a description of the C.D.W. transition in the 2H layered compounds, ascribing to 2H TaSe<sub>2</sub> exemplary status, are:

Electronic     $\omega_c = .6 \text{ eV}$   
                    $N = 1, 1.1, 1.2, 1.3$

4-12

Phonons         $W_o = 0, .1$   
                    $2 A_{1g}$  modes at  $T=0$ : 10.1 meV, 5.46 meV  
                    $2 E_{2g}$  modes at  $T=0$ : 8.06 meV, 6.2 meV  
                    $G_{i/3}$  L.A. (A) phonon at  $T_c$ : 5 meV

Electron/Phonon Coupling     $g' = \frac{6m_o\omega_q^2}{g^2} = 2.2 - 3.0$

Proceeding with the numerical calculations of the thermodynamics implied by these parameters in the context of the saddle point model, on a mesh a size;

$$0 \leq v \leq .2 \omega_c \text{ intervals of } .01 \omega_c$$

4-13

$$0 \leq kT \leq .1 \omega_c \text{ intervals of } .01 \omega_c$$

The free energy  $F(N, T, \Delta)$  and  $\left(\frac{\partial F}{\partial \Delta}\right)_{N, T}$  are evaluated. The constraint of constant electron number  $N$  requires that the chemical potential  $\mu(\Delta, T)$  at each  $(v, T)$  mesh point satisfy the condition

$$N = \frac{8}{\pi} \sum_{i=1}^3 \int_0^{\pi/6} d\theta \int_0^{1/2} \frac{dK}{(e^{\beta(E_i - \mu)} + 1)} = 1 - \frac{4}{\pi} \sum_{i=1}^3 \int_0^{\pi/6} d\theta \int_0^{1/2} dK \tanh\left(\frac{\beta(E_i - \mu)}{2}\right)$$

4-14



This constraint is effected by determining electron number  $N$  at each  $(v, T)$  mesh point for a range of chemical potential values followed by a least square program to interpolate to the chemical potential appropriate for the desired  $N$  value.

With the values for  $F(N, T, \Delta)$  and  $\left. \frac{\partial F}{\partial \Delta} \right)_{N, T}$  calculated at each mesh point, the solution to  $\left. \frac{\partial F}{\partial \Delta} \right)_{N, T} = 0$  subject to the constraint  $(F^\Delta - F^0) < 0$  and  $0 \leq v < +.2\omega_c$  is realized by solution to a quadratic fit to  $\frac{\partial F}{\partial \Delta}$  in the region where it changes sign. Where the transition temperature  $T_c$  exists for  $T_c < .1\omega_c$ , a least square interpolation program isolates this point and the corresponding electronic gap in the situation of a first order transition. The two dimensional electronic momentum space integrals, which form the core of the numerical work, are evaluated by means of Gaussian quadrature.

### 4.3 Numerical Results

The previous section established the electronic and lattice parameters appropriate to a discussion of the C.D.W. phase transition. In this section, results of numerical calculations are given where the emphasis is upon correlating experimental observations with trends established within the parameter regime pertinent to the saddle point model.

Fig. 4.2 depicts the zero temperature energy gap solution for variations in  $N$  and  $g'$ . As the phonon zero point energy is suppressed by at least an order of magnitude relative to the lattice distortion energy, these zero temperature results are

independent of  $W_0$ . For given  $N$ , as  $g'$  increases, the condition that  $(F^\Delta - F^0) < 0$  causes eventual termination of the line of acceptable solutions, except for  $N = 1$  where the saddle point singularity structure guarantees a solution for any  $g'$ . For  $N < 1$ , the condition of electron-hole symmetry results in the solution for  $N$  being identical to  $(2-N)$ .

For given  $g'$ , the dependence of  $N$  upon the electronic gap illustrates a novel and experimentally relevant feature implicit in the saddle point model. As the saddle point is depressed below the Fermi level by increasing  $N$ , only by increasing the electronic gap can access to this region of high density of states be achieved. As the condition realized in the 2H compounds is that of the  $\Gamma$ -K saddle points situated below the Fermi level, the increase in electronic gap with electronic concentration  $N$  corroborates with the relatively large energy of .25 eV which Barker et al<sup>20</sup> observed in the absorption spectrum of 2H TaSe<sub>2</sub> in the C.D.W. state.

Translating the .25 eV energy absorption into the energy gap value employed in model calculations, requires recognition that the cubically coupled energy bands, initially degenerate at the saddle point, are split into bands with energies of  $(-2v, +v, +v)$  for  $N > 1$  at the saddle points. In addition, the logarithmic density of states singularity is maintained in the C.D.W. state but contained in one of the depressed energy bands at an energy essentially equal to  $-v$

and only slightly displaced from its initial saddle point position in momentum space. Thus, the anticipation is that optical transitions from the high density of states region of the lower band at energy  $-v$  to states of the upper band, totally unoccupied for  $N < 1.33$ , at energy  $+2v$  constitute the major new absorption feature of the C.D.W. state.

Attributing the .25 eV absorption to excitation across a  $3v$  gap, the electronic gap is established at:

$$3v = .25 \text{ eV}$$

$$v = .08 \text{ eV}$$

Using  $\omega_c = .6 \text{ eV}$  for the bandwidth, the energy gap pertinent to .08 eV is  $v = 14$ , expressed in units of  $10^{-2} \omega_c$ . As discussed in the previous section, an energy of .08 eV taken together with the value of  $g \sim 3$  inferred from  $T > T_c$  electronic and phonon characteristics favorably correlates with the observed zero temperature lattice distortion of  $\sim .05 - .09 \text{ \AA}$ .

For finite temperature, Fig. 4.3, with  $W_0 = 0$ , displays the characteristics of the purely electronically driven transition where, except for  $N = 1$  where the transition is second order, the phase transition becomes progressively more first order with increasing  $N$ . For a given  $g$  value, increasing  $N$ , though producing an increasing zero temperature gap value, results in a lowering of the transition temperature  $T_c$ . This

is attributable to the progressive instability of the gap produced by increasing  $N$  at fixed  $g$  against entropy accrument.

To achieve the experimentally realized transition temperature of 120K or  $T_c = 1.8$  in units of  $10^{-2} \omega_c$  with  $\omega_c = .6$  eV, the set ( $N = 1.3, g' = 2.8$ ) offers a plausible energy gap against temperature spectrum. Referring to table 4.1 and table 4.2 for a compilation of susceptibility and specific heat discontinuity results, for  $W_0 = 0$ , the susceptibility results align well with experiment while the specific heat values, though tenable over a range of  $N$  and  $g'$  with experimental results, fails by approximately an order of magnitude for ( $N = 1.3; g' = 2.8$ ), the case of interest.

Turning to Fig. 4.4, the influence of the weight factor  $W_0$  upon the energy gap's temperature dependence is displayed. The thermodynamic influence of  $W_0$ , as the factor multiplying the phonon free energy difference

$$(F^\Delta - F^0) = W_0 kT \left[ \sum_{i=1}^6 \log (1 - e^{-\beta \hbar \omega_{G/3}^i}) - 6 \log (1 - e^{-\beta \hbar \omega_{G/3}^0(T_c)}) \right]$$

4-15

is dependent upon the C.D.W. phonon spectrum, determined by the  $\omega_{G/3}(T, \Delta)$ 's, relative to the phonon frequency at  $T_c$ ,  $\omega_{G/3}^0(T_c)$ . As the mean zero temperature C.D.W. phonon energy is  $\sim 7.4$  MeV compared with the  $T_c$  phonon energy of  $\sim 5$  MeV, the C.D.W. state lowers phonon entropy and thus assists the electronic entropy in driving the C.D.W. transition, for a given ( $N, g$ ), to  $T_c$  values reduced from those of the  $W_0 = 0$

situation. As Tables 4.1 and 4.2 indicate, while increasing  $W_0$  to finite values leaves the susceptibility essentially unchanged, its enhancement of the specific heat discontinuity produces numerical equality with the observed experimental results for  $W_0 \approx .06 - .1$ . Due to limitations of mesh increments of  $.01 \omega_c$ , calculation of specific heat, based upon polynomial fit to calculated entropy values, becomes unavailable for  $T \leq .04 \omega_c$ , and recourse to established trends is invoked.

The weak dependence of the susceptibility difference  $\chi(T_c) - \chi(0)$  for  $N \geq 1.1$  emerges from two influences. First,  $\chi(0)$  is essentially independent of  $W_0$  for  $W_0 \leq .5$  as lattice zero point energy is small compared to the distortion energy. Second, as  $N$  increases from  $N=1$ , where the susceptibility diverges logarithmically at  $T=0$ , variations in susceptibility in the vicinity of  $T_c$  are relatively small. Fig. 4.5 displays characteristic susceptibility features of the saddle point model.

Taken as a whole, these numerical calculations strongly support the saddle point model as the key electronic agent in the 2H C.D.W. phase transition, correlating the observed zero temperature electronic gap/lattice distortion with the observed partial softening of the  $q = G_1/3$  L.A. phonon and producing a susceptibility difference  $\chi(T_c) - \chi(0)$  comparing favorably with experiment. Also, given the large ratio  $v(0)/kT_c \approx 15$ , model predictions of this ratio are realized by displacing the  $\Gamma$ -K saddle points below the Fermi level, where band structure calculations would place them.

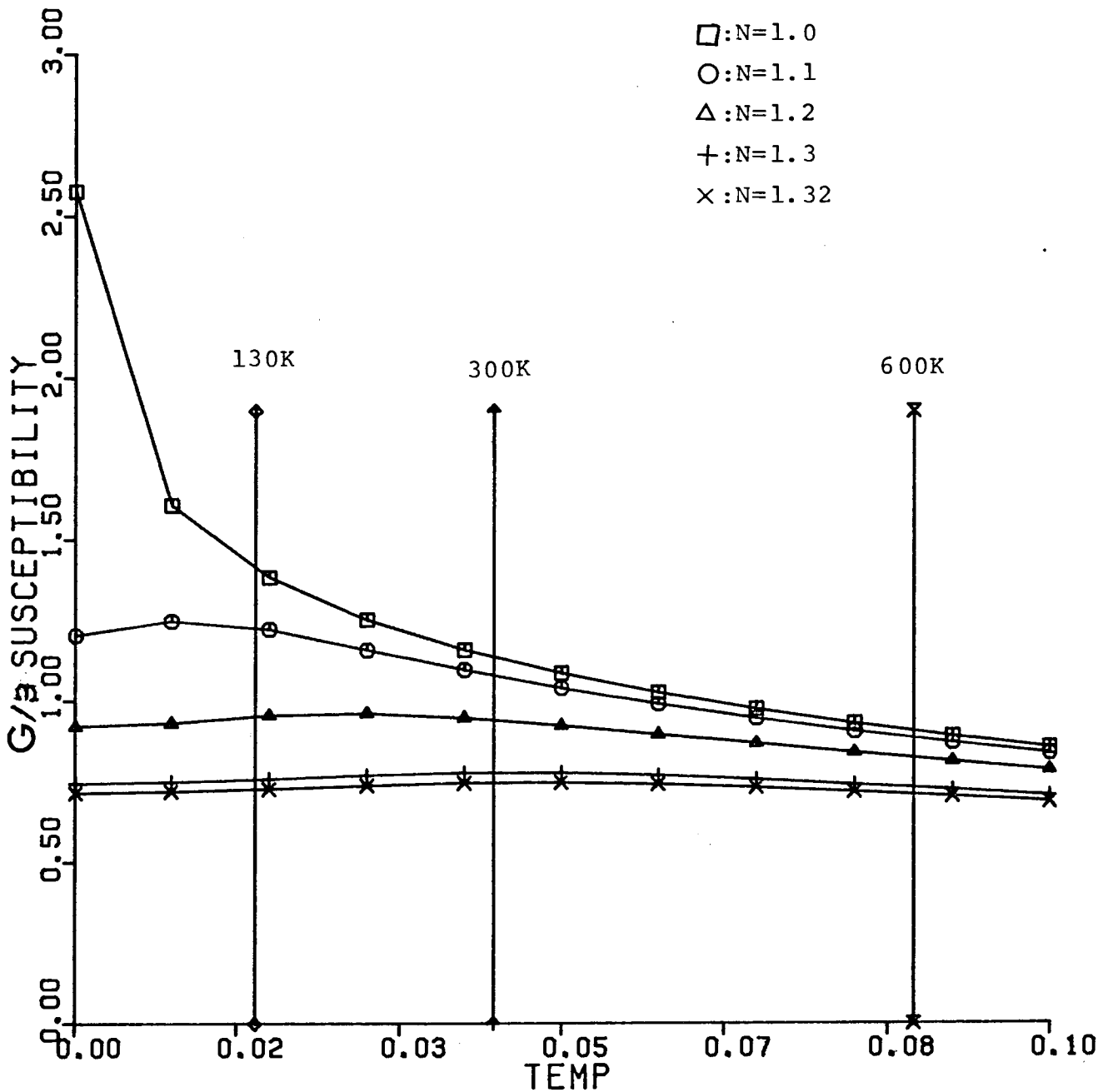


Fig. 4.1:  $G/3$  normal state susceptibility for various  $N$  values. The temperature is in units of  $10^{-2}\omega_c$ . Susceptibility in units of  $\omega_c^{-1}$ . The temperatures indicated assume that  $\omega_c = 0.6\text{eV}$ . For  $N=1.$ , divergence is logarithmic at  $T=0$ .

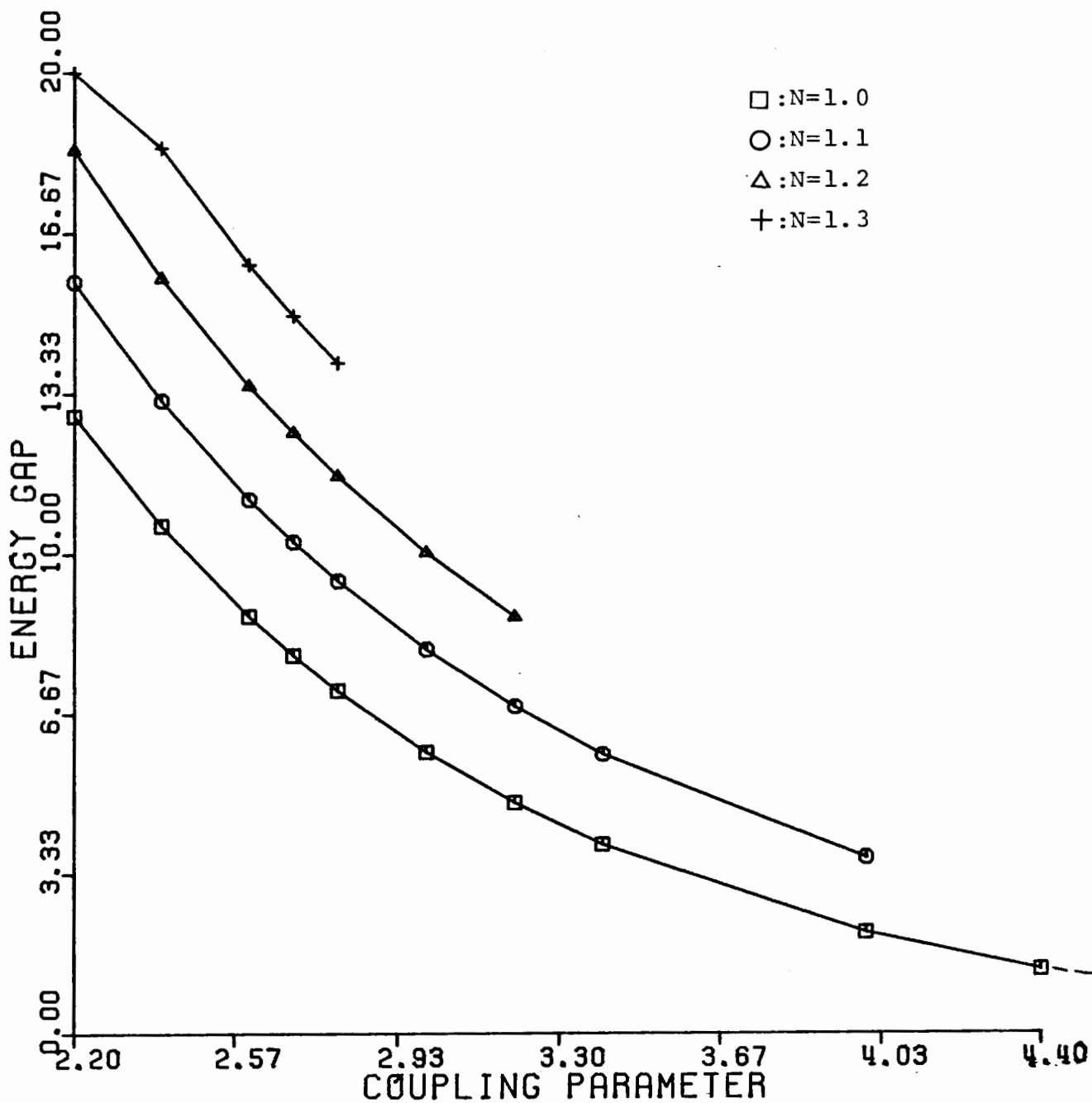


Fig. 4.2:  $T=0$  solutions for the electronic energy gap for various  $N$  values. Energy gap is in units of  $10^{-2}\omega_C$ . For  $N=1.0$ , solutions exist for all values of the coupling parameter. For  $N=1.1, 1.2, 1.3$ , line of solutions terminates as coupling parameter increased beyond some critical value.

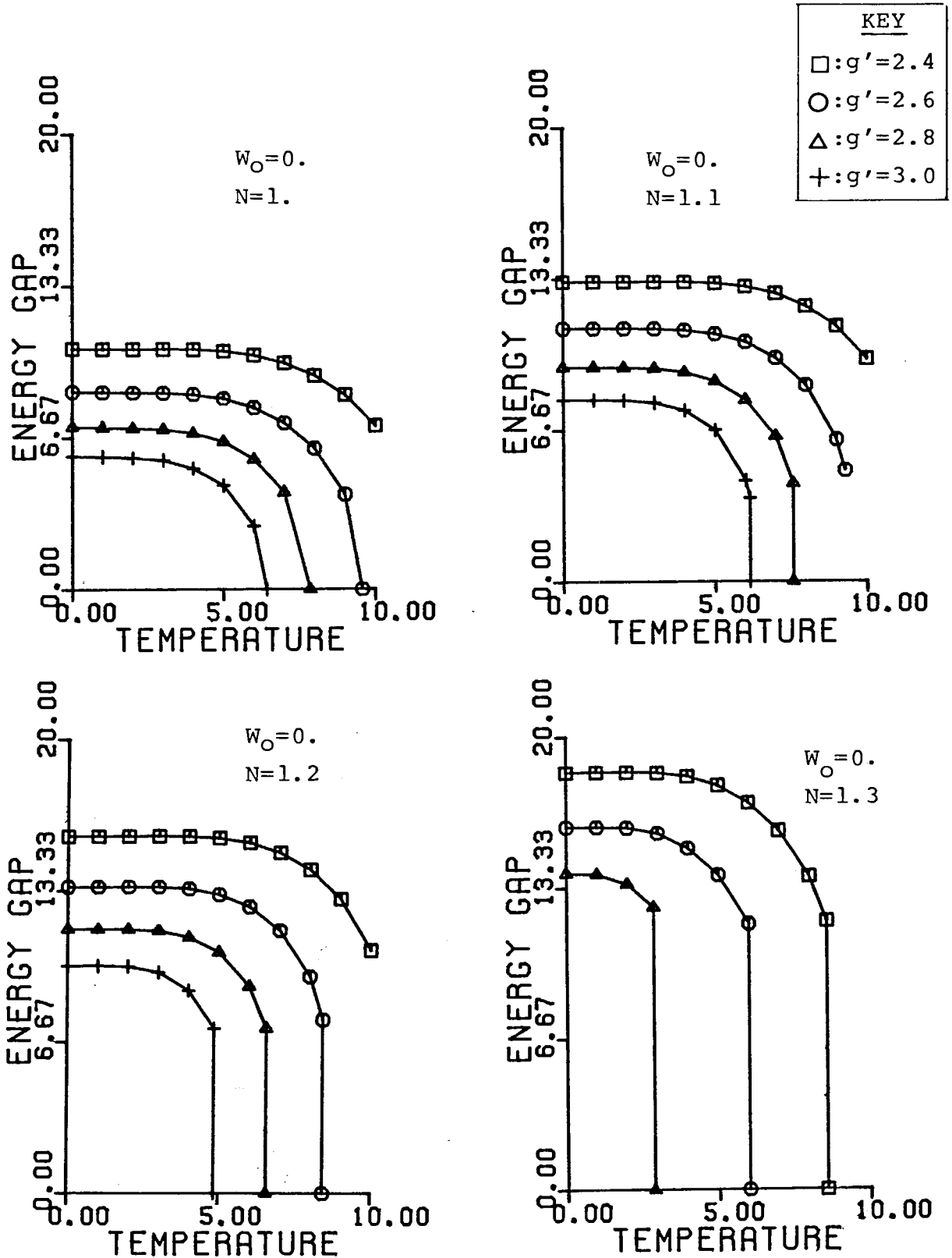


Fig. 4.3:  $W_0 = 0$  electronic energy gap for various  $(N, g')$  values. Temperature and energy gap in units of  $10^{-2} \omega_C$ . Note increase in  $\Delta(0)$  and decrease in  $T_c$  as  $N$  increased.



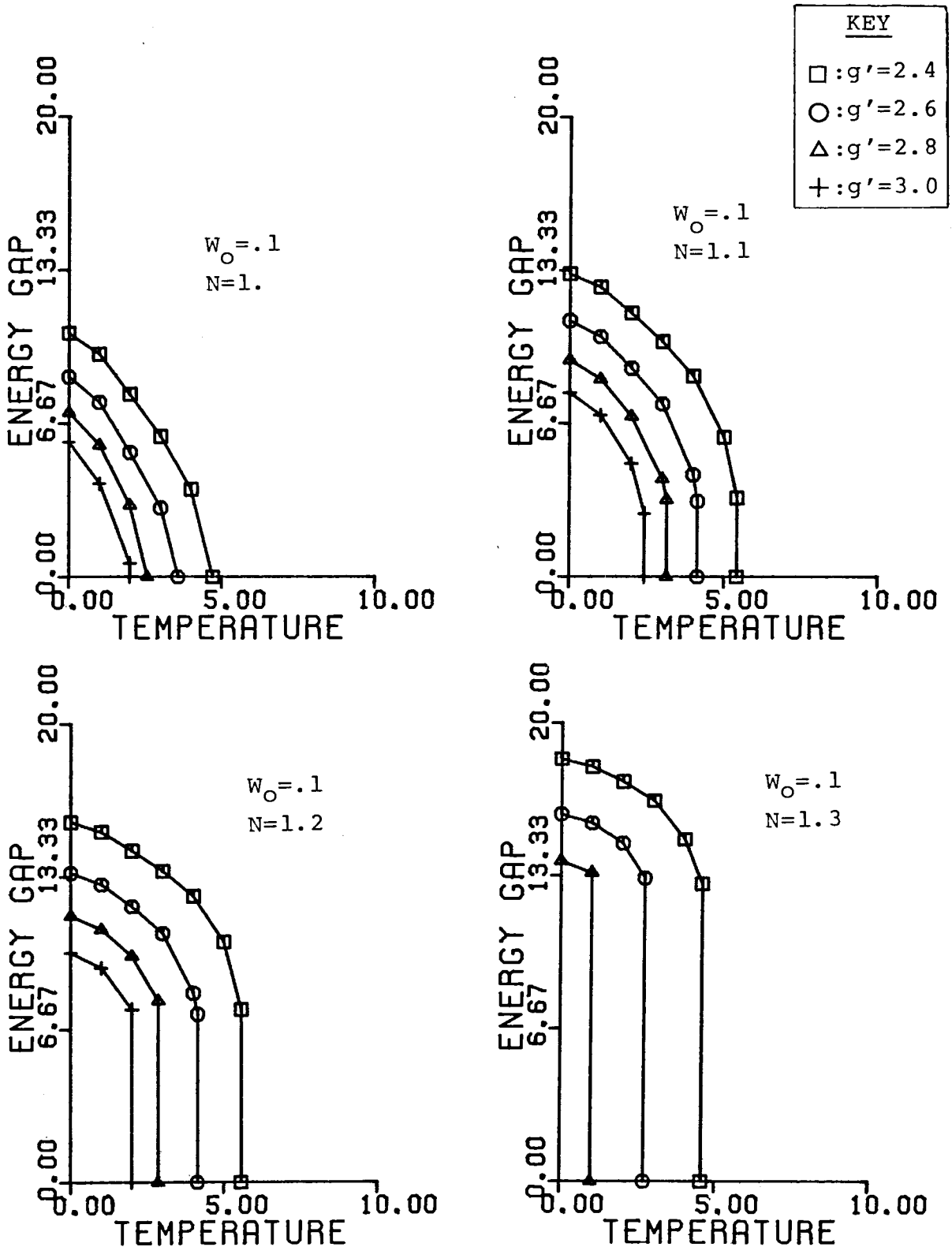


Fig. 4.4;  $W_0 = 0.1$  electronic energy gap values for various  $(N, g')$  values. Temperature and energy gap in units of  $10^{-2} \omega_c$ . Note depression of  $T_c$  relative to  $W_0 = 0$  values.

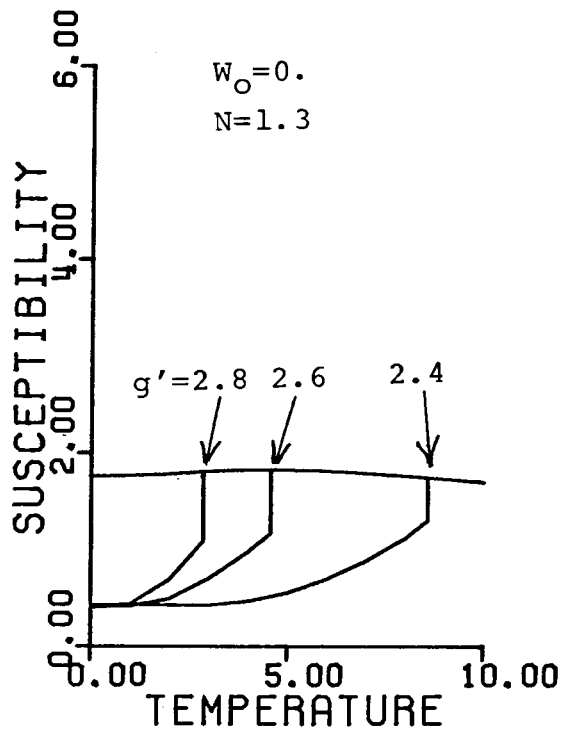
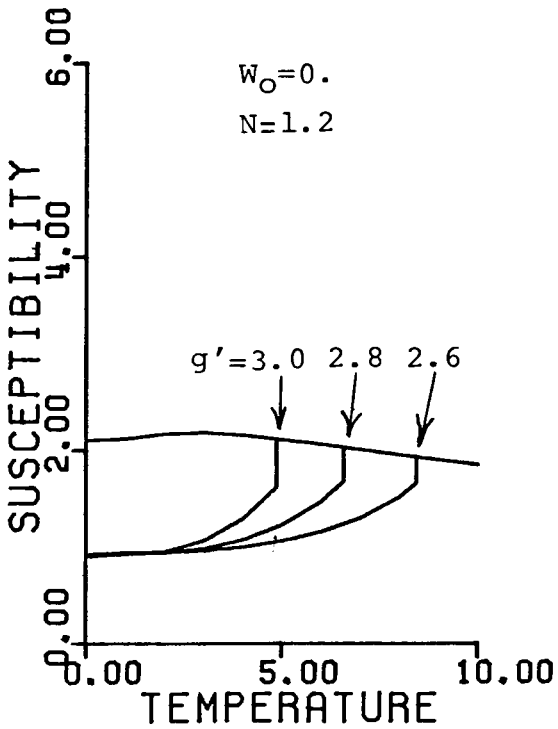
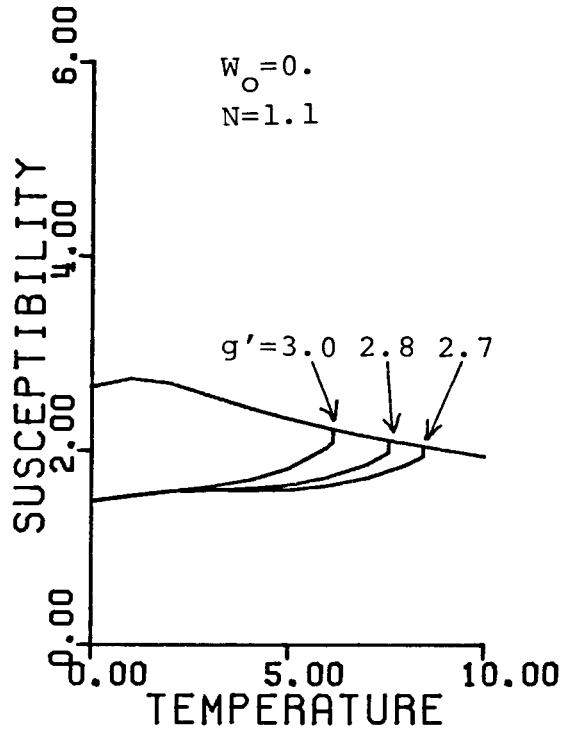
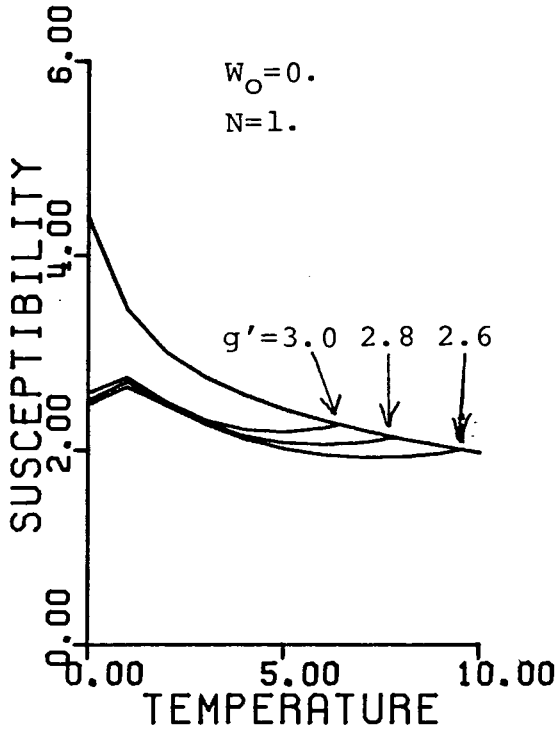


Fig. 4.5: Composite of normal state susceptibility defined as  $\Delta=0.$  solution with C.D.W. susceptibilities generated from various  $(N, g')$  values. Temperature in units of  $10^{-2} \omega_c.$  Multiplication of susceptibility by  $u_B^2/\omega_c$  reproduces values of Table 4.1 for  $W_0=0.$

Table 4.1 - Electronic Susceptibility

The bare magnetic spin susceptibility is defined by:

$$\chi(T) = \lim_{q \rightarrow 0} \frac{\mu_B^2}{\omega_c} \cdot \frac{8}{\pi} \sum_{i=1}^3 \int_0^{\pi/6} d\theta \int_0^{0.5} dk \frac{f(E_K^i) - f(E_{K+q}^i)}{E_{K+q}^i - E_K^i}$$

$$\chi(T) = \frac{\mu_B^2}{\omega_c} \cdot \frac{2}{\pi T} \sum_{i=1}^3 \int_0^{\pi/6} d\theta \int_0^{0.5} dk \frac{1}{\cosh^2\left(\frac{E^i - \mu}{2kT}\right)}$$

Tabulating the quantity  $\chi(T_c) - \chi(0)$  in units of  $10^{-6}$  emu/mole (for  $\omega_c = .6$  eV)

$g' =$	2.4	2.6	2.7	2.8	3.0
N = 1.		-23.7	-21.	-18.	-15.6
1.1				38.2	45.2
1.2		60.3	63.7	66.3	72.2
1.3	73.8	77	78.7	78.1	
1.32	80.	80.3	79.2		

$W_0 = 0.$

$g' =$	2.2	2.4	2.6	2.8
N = 1.	-7.	-1.	8.62	16.7
1.1	34.4	43.1	51.9	57.
1.2	55.5	61.4	64.1	66.2
1.3		74.	72.7	

$W_0 = .1$

Experimentally:  $\Delta\chi = 55 \times 10^{-6}$  emu/mole for 2H TaSe<sub>2</sub>

Table 4.2 - Specific Heat Discontinuity

From the calculated value of  $\Delta(T)$ , the entropy is given by:

$$S(\Delta, T, N) = -\left(\frac{\partial F}{\partial T}\right) = S_{el} + S_{ph}$$

$$S_{el} = \frac{k_B}{\pi\alpha} \sum_{i=1}^3 \int_0^{\pi/6} d\theta \int_0^{0.5N, \Delta} dk \left[ \frac{(E_i - \mu)}{KT} \cdot \frac{1}{e^{\beta(E_i - \mu)} + 1} + \log(1 + e^{-\beta(E_i - \mu)}) \right]$$

$$S_{ph} = k_B \cdot W_0 \sum_{i=1}^6 \left[ \frac{\hbar\omega_i}{k_B T} \cdot \frac{1}{e^{\beta\hbar\omega_i} - 1} - \log(1 - e^{-\beta\hbar\omega_i}) \right]$$

From a least square polynomial fit to the entropy

$$S(T) = X(1)T + X(2)T^2 + X(3)T^3 + X(4)T^4$$

the specific heat at constant value is obtained:

$$C_V = T \cdot \left(\frac{\partial S}{\partial T}\right)_N = X(1)T + 2X(2)T^2 + 3X(3)T^3 + 4X(4)T^4$$

The specific heat discontinuity at  $T_c$  is given as the difference between normal and C.D.W. state specific specific heat. All tabulated values are in units of  $k_B$  per Ta atom:

$W_0 = 0.$						$W_0 = .1$				
	2.4	2.6	2.7	2.8	3.0		2.2	2.4	2.6	2.8
N=1.	-	.25	.33	.36	.38	N=1.	1.2	1.24	-	-
1.1	-	-	.37	.44	.49	1.1	1.75	1.57	1.4	.8
1.2	-	.27	.45	.50	.63	1.2	1.78	1.7	1.	-
1.3	.06	.14	.27	.61	-	1.3	-	-	-	-

Experimentally:  $\Delta C_V \approx .48 k_B$  per Ta atom (Craven et al<sup>21</sup>)

### 5.1 Fermi Surface Topology

In this final chapter, discussion is directed to two rather diverse issues of the 2H C.D.W. phase which as yet lack full understanding. First, as treated in this section, is the nature of the electronic band structure in the C.D.W. state as probed by the de Haas-van Alphen experiment of Graebner<sup>18</sup>. Second, treated in the following section, is the C.D.W. normal mode structure.

As the band structure calculations of Mattheiss indicated, the Fermi surface of the 2H structure consists essentially of cylindrical sections running parallel to the c-axis and centered about the  $\Gamma$ -K points. Measurement of a positive Hall constant<sup>24</sup> is in accordance with the hole-like character of these cylindrical regions.

The de Haas-van Alphen results of Graebner<sup>18</sup>, as discussed in Chapter 1, indicate four orbits per conduction band in the C.D.W. state of 2H TaSe<sub>2</sub>. Using a band structure reorganization dictated by the  $\Gamma$ -K saddle point coupling model, Fig. 5.1 qualitatively illustrates the resulting C.D.W. Fermi surface. Noteworthy are the resulting four orbits, in agreement with the de Haas-van Alphen results. Also, three of the four orbits are electron like, consistent with the reversal of Hall coefficient<sup>25</sup> from positive to negative in the C.D.W. phase.

To understand how this Fermi surface emerges from the  $\Gamma$ -K saddle point coupling reference to Figures 3.1 and 3.2 is helpful. The cubic saddle point coupling mixes electronic "bands" (4,5,9) and (4,5,8), where the Fermi surface of bands 4 and 8 contains both C.D.W. "active" (close to saddle point) and "inactive" (removed from saddle point) portions. Given the (+2v, -v, -v) saddle point splitting appropriate for the  $N > 1$  situation, coupling of bands (4,5,9) results in band 9 assuming the +2v value and accordingly pushed entirely above the Fermi energy while band 4 and 5 are depressed in energy. Thus, as Figure 5.1 illustrates, in the C.D.W. state, band 9 is completely empty while 5 remains totally occupied.

In passing from the (4,5,9) coupling region to the (4,5,8) coupling region, the C.D.W. electronic energy value derived from band 4 in the (4,5,9) region is associated with band 8 in the (4,5,8) region while the energy eigenvalue derived from band 9 in the (4,5,9) region is associated with band 4 in the (4,5,8) region. This band "cross-over" couples the Fermi surface of band 4 in the (4,5,9) region to that of band 8 in the (4,5,8) region to produce the isolated hole pockets along  $\Gamma$ -M in one of the (4,8) reduced zones. On the other hand, the coupling of the "inactive" Fermi surface of band 8 with the "active" portion originally associated with band 4 in conjunction with the +2v saddle point elevation of this band, produces the K-point electron pocket configuration of the other (4-8) reduced zone.

This mixing of electronic energies from the undistorted state to qualitatively generate a C.D.W. Fermi surface agreeing with the de Haas-van Alphen as well as Hall constant data is strong evidence for the applicability of the saddle point model. As an alternate explanation of this data, Wilson<sup>26</sup>, using a Fermi surface constructed from the 2H band structure results of Wexler and Woolley<sup>8</sup> and with C.D.W. coupling phenomenologically introduced principally amongst the K point cylinders, deduces a C.D.W. Fermi surface structure resulting in five orbits. Thus a fortuitous degeneracy in the extremal area of two Fermi surfaces is required before agreement with experimental data is achieved.

## 5.2 The Raman Active C.D.W. Modes

Given the commensurability existing between lattice and C.D.W. periodicity in the 2H layered dichalcogenides, it is possible to construct representations for the C.D.W. normal modes (phonons) as a finite linear superposition of normal modes from the undistorted state. Assuming that only modes from a given branch are coupled by the C.D.W. distortion, the  $G_{i/3}$  C.D.W. distortion in the 2H system results in C.D.W. normal mode coordinates expressible as a superposition of nine modes from the undistorted phase.

As discussed, the six L.A. (A)  $q = G_{i/3}$  normal modes of the undistorted state, by virtue of their coupling to longitudinal electronic fluctuations at  $q = G_{i/3}$ , are the principal lattice modes participating in the C.D.W. transition. These

six equivalent modes, together with the two K-point and single zone center modes, form a representation for nine  $q=0$  modes in the reduced C.D.W. zone with reciprocal lattice vector  $G_i/3$ . Given the energy separation between these three distinct regions, the six modes belonging to the star of  $G_i/3$  essentially exist as a self coupled subspace independent of zone center and K point influences and form a basis for the C.D.W. lattice modes.

The Raman work of Holy et al<sup>15</sup> showed that the modes appearing in the C.D.W. state were consistent with an even parity triple- $q$  C.D.W. state, though their use of the full  $D_{6h}^4$  crystal symmetry required both layers of the unit cell to explain the number and symmetry of the observed C.D.W. lattice modes. As shown in Chapter 2, neglecting interlayer interactions leads to a  $D_{3h}$  symmetric single layer treatment of the C.D.W. lattice modes. The original six L.A. A modes from the star  $q=\pm G_i/3$  when mapped to  $q=0$  in the C.D.W. state transform as two  $A_1$  and two  $E'$  representations of the  $D_{3h}$  layer symmetry. Since the  $A_1$  and  $E'$  modes are Raman as well as infra-red active, the observed C.D.W. Raman spectrum of two A and two E symmetric modes can be viewed as a natural expression of the  $D_{3h}$  layer symmetry. Note, as the Raman scattering tensors for  $D_{3h}$  and  $D_{6h}$  are identical, Raman scattering measurements do not distinguish between these two symmetry types.

In the context of the proposed microscopic Hamiltonian, the six L.A. A modes couple in the C.D.W. state via a Bragg scattering mechanism generated by the anharmonic term. The



resulting  $q=0$  C.D.W. lattice normal modes become strongly split about a frequency renormalized by the electron-phonon term. Their frequency dependence upon the C.D.W. distortion amplitude emerges directly from the diagonalization of a  $6 \times 6$  matrix equation, as expressed in equations 2.38, 2.40, and 2.41.

A major feature of this interpretation is the existence of a fixed splitting ratio separating the C.D.W. modes. Figure 5.2 displays the observed C.D.W. frequency dependence taken from Steigmeier et al<sup>22</sup> and Irwin<sup>23</sup> with those anticipated by model calculations. Using the experimentally determined mode frequencies at  $T = 0$  and  $T = T_c$  as given boundary conditions, model calculations of the ratio  $\Delta(T)/\Delta(0)$  determines the intervening C.D.W. mode frequencies. As the ratio  $\Delta(T)/\Delta(0)$  is relatively insensitive to the particular  $[N, g']$  parameter set from which it is generated, the model dispersion result illustrated in Figure 5.2 is characteristic of anharmonic coupling influences rather than an artifact of the  $[N, g']$  parameters.

General agreement between model and experimental results is evident from Figure 5.2, especially in the low temperature regime. As this thesis does not consider complications introduced by incommensurate effects, model frequency behavior near the transition temperature is only suggestive.

In closing, it is perhaps informative to compare this split mode interpretation with the more usual "phase" and "amplitude" mode description which views the C.D.W. normal modes as phase

and amplitude displacements of the C.D.W. lattice with respect to the host lattice. Using the phase and amplitude mode description, Holy et al<sup>15</sup> argued that the lower lying ( $A_{1g}, E_{2g}$ ) set be equated with the phase modes while the more energetic ( $A_{1g}, E_{2h}$ ) set be equated with the amplitude modes. However, as the work of Steigmeier et al<sup>22</sup> revealed, the lower  $E_{2g}$  mode exists well into the incommensurate phase at finite frequency which is contrary to the expected phase mode behavior<sup>19</sup> of approaching zero frequency as the transition temperature is approached from below. This throws into question the applicability of phase and amplitude characterization of these observed C.D.W. modes. As Steigmeier notes, in the undistorted phase ( $T > T_c$ ), a broad feature at about  $130 \text{ cm}^{-1}$  (2H TaSe<sub>2</sub>) develops which is ascribed to two phonon scattering by the  $q = G_1/3$  L.A.(A) modes whose frequency corresponds to that obtained from the neutron work of Moncton et al<sup>13</sup>. It would seem natural to associate the new frequencies observed in the C.D.W. state as emerging from this precursor two phonon peak but strongly split by Bragg scattering influences.

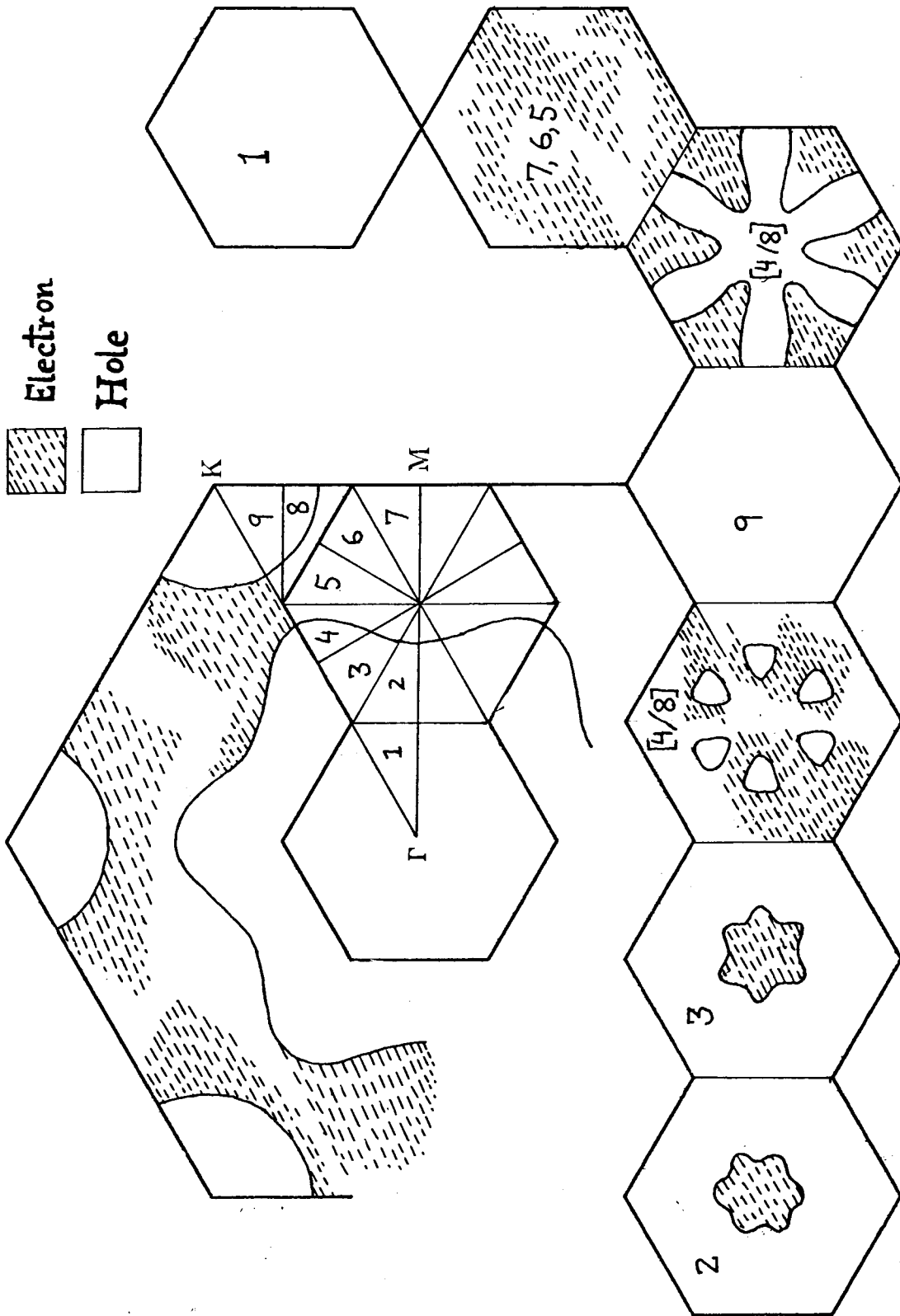


Fig. 5.1:  $\vec{G}/3$  remapping of normal state full zone by the C.D.W. distortion. Illustrated Fermi surfaces are qualitative. Compare this C.D.W. electronically modified situation with the undistorted situation of Fig. 3.1

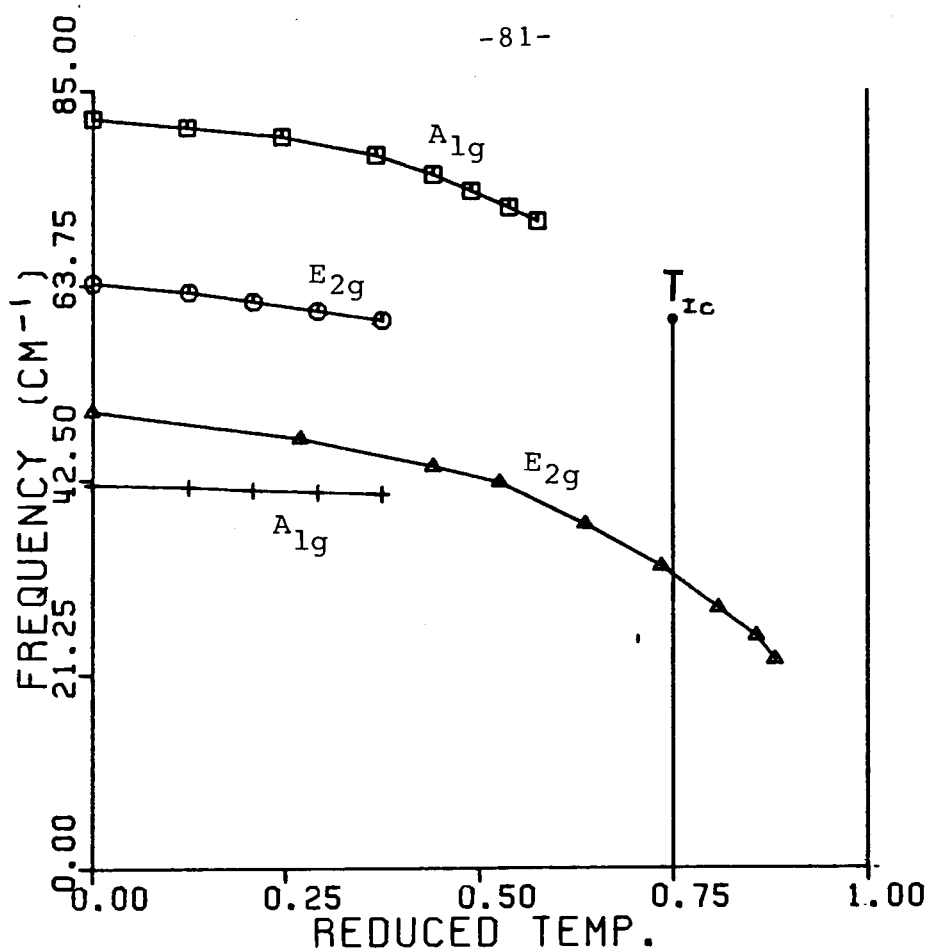


Fig. 5.2a: Experimental values of the Raman active C.D.W. modes. Note how the lower E<sub>2g</sub> mode exists into the incommensurate C.D.W. phase. From ref. 22 and 23.

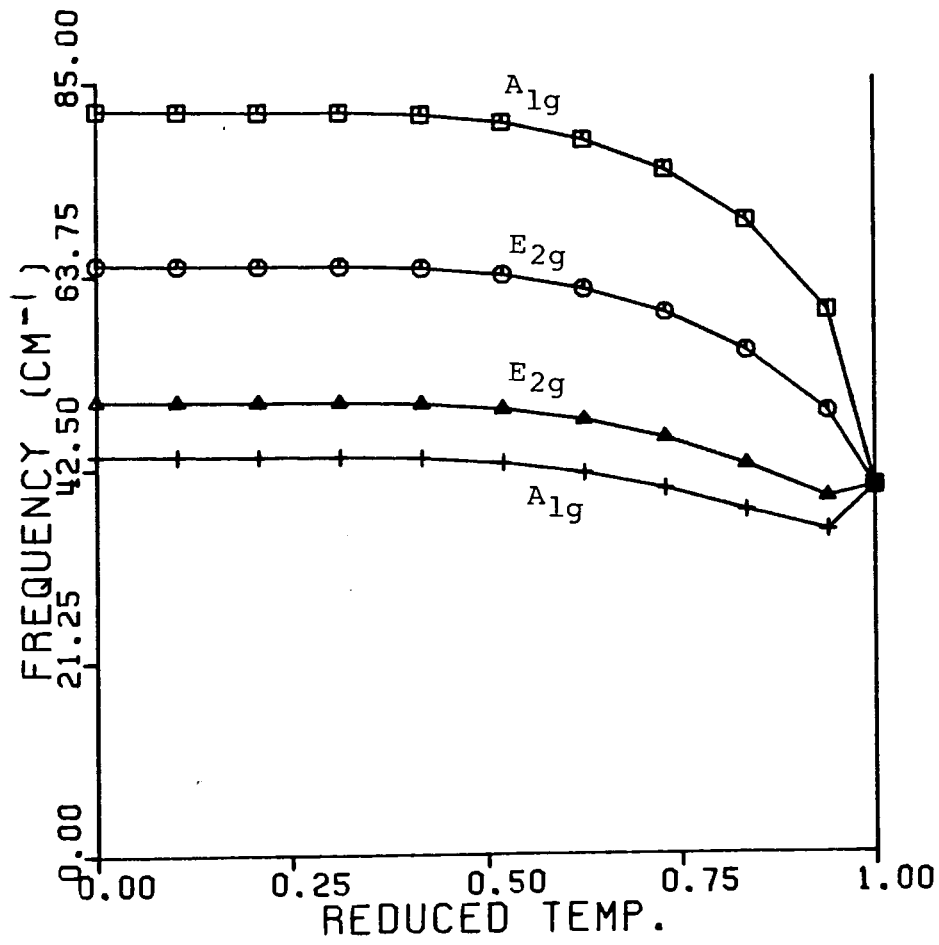


Fig. 5.2b: Mode splitting behavior of the Raman active C.D.W. modes predicted from the model Hamiltonian.

APPENDIX A

COMPUTER ROUTINES

The basic numerical format was outlined in Chapter 4. In this appendix, two computer programs characteristic of the essential numerical processing are reproduced.

The first program (program Gaussian) is a 12-point Gaussian integration routine designed to integrate a function  $F(\theta, k)$  over the two dimensional electronic Brillouin zone. Usual formatting conditions specified for the decomposition of the k-space area into 12 regions with evaluation at 144 points in each region. Essential for numerical accuracy was to incorporate the Fermi surface into the set of boundary points between different regions. By integrating various known functions or increasing the number of integration regions, the numerical accuracy is assessed at better than 1%.

The second program (program Least Square), taking results from the integration routine as input data, determines the electronic gap which minimizes the total free energy at a given temperature. Essential to this program, as well as program Gaussian, are package programs available from IMSL. In this instance, program LLSQF calculates the least square coefficients used in the polynomial fit to the free energy in the vicinity of its local minimum.

```
//ACXBELLN JOB (****,****),SCOTT,MSGCLASS=R,TIME=10
//PORTRAN EXEC PORTGCG
  DIMENSION R2(40),V3(40)
  DIMENSION FR(70),TOT1(80),TOT2(80),TOT3(40),TOT4(40),
C TOT5(40),TOT6(40),TOT7(40)
  DIMENSION U2(40),V2(40),U4(231),FRL(40)
  DIMENSION C11(13),T11(13)
  DIMENSION GW(12),GP(12)
  DIMENSION HP(12),HW(12)
  DIMENSION C1(13),T1(13)
  DIMENSION CU(12),CU1(12)
  DIMENSION TT(4),WT(4)
  EXTERNAL FGO
  COMMON T,U,V,R,AD1,AD2,AD3,EUP,ELO,CC,A
  PI=3.14159265
  NGU=12
  NGUU=12
  SCAL=100.
  ANN=1.37
  A=0.0
  AA=1./((1.-A)*2.)*SCAL
C FOR A GIVEN ELECTRONIC CONCENTRATION, THE CHEMICAL
C POTENTIAL CORRESPONDING TO A GIVEN RANGE OF
C ELECTRONIC GAPS AND TEMPERATURES IS INPUTED
  DO 600 JR=1,33
  J1=(JR-1)*7+1
  J2=J1+6
  READ(5,606) (U4(LP),LP=J1,J2)
606 FORMAT(7F8.5)
600 CONTINUE
  NX=5
  NN=11
C THE FREE ENERGY FOR A RANGE OF TEMPERATURES (NV)
C AND ELECTRONIC GAPS (L) IS CALCULATED
  DO52 NV=1,11
  R=R2(NV)*SCAL
  NZ=(NV-1)*21+1
  UXX=U4(NZ)*SCAL
  DO50 L=1,21
  V=V2(L)*SCAL
  LXX=(NV-1)*21+L
  U=U4(LXX)*SCAL
  AD1=1.
  AD2=V*V/AD1/AD1
  AD3=V*V*V/AD1/AD1/AD1
  AD=AD1
C THE INTEGRATION LIMITS FOR THE 12 POINT GAUSSIAN
C QUADRATURE METHOD ARE ESTABLISHED (CU(1),...,CU(6))
  CC=1.
  EUP=2.*V
  ELO=-V
  IF(CC.LT.0.) EUP=V
  IF(CC.LT.0.) ELO=-2.*V
```

```
ZZ=1.*CC
B=(4.*A+ZZ)*(4.*A+ZZ)
P=((6.*ZZ*CC*B-54.*ZZ*CC)-SQRT((6.*B-54.)*(6.*B-54.))
C -4.*(9.*B-81.)*(9.*B-9.))/2./(9.*B-81.)
E=2.*A*P+(P*ZZ+CC-ZZ*SQRT(9.*P*P-6.*ZZ*CC*P+9.))/2.
EM1=E*V
P=P*V/AD1
IF(U .GT. EM1 .AND. CC .LT. 0.) GOTO13
IF(U .LT. EM1 .AND. CC .GT. 0.) GOTO13
AL=(V+U*CC)/(1.+2.*A*CC)
GOTO14
13 QR=-6.*CC*ZZ*(4.*A+ZZ)*(2.*U/V-CC)-72.+9.*(4.*A+ZZ)*(4.*A+ZZ)
C +9.*(2.*U/V-CC)*(2.*U/V-CC)
QR=SQRT(QR)
AL=((4.*A+ZZ)*(2.*U/V-CC)-3.*CC*ZZ-QR)/((4.*A+ZZ)*(4.*A+ZZ)-9.)
AL=AL*V/AD1
B1=(2.*A+2.*CC)*V*CC-U*(4.*A+CC)
B2=(2.*A+2.*CC)*(2.*A-CC)
B3=U*U-U*V*CC-2.*V*V
A6=(-B1-SQRT(B1*B1-4.*B2*B3))/(2.*B2)
14 N4=1
IF(U .LT. EM1 .AND. U .GT. ELO .AND. CC .LT. 0.) N4=-1
IF(U .GT. EM1 .AND. U .LT. EUP .AND. CC .GT. 0.) N4=-1
17 SHEL=4.
IF(U .GT. ELO .AND. U .LT. EUP) NR=3
IF(U .LT. ELO) NR=1
IF(U .GT. EUP) NR=5
UO=UXX
AL1=UO/(AD1*2.*(A-1.))
IF(UO .GT. 0.) AL1=UO/(AD1*2.*(A+1.))
IF(AL1 .LT. .0001) AL1=.0001
IF(AL .LT. .0001) AL=.0001
S=AA
NGG=1
IF(AL .GE. S) NGG=-1
IF(AL .GE. S) AL=S
CU(1)=0.0
CU(3)=AL
CU(4)=AL+(S-AL)/4.
CU(5)=AL+(S-AL)/2.
CU(6)=S
CU1(1)=0.
CU1(2)=AL1
CU1(3)=AL1+(S-AL1)/4.
CU1(4)=AL1+(S-AL1)/2.
CU1(5)=AL1+(S-AL1)*3./4.
CU1(6)=S
DO45 KV=1,13
C1(KV)=0.
T1(KV)=0.
T11(KV)=0.
C11(KV)=0.
45 CONTINUE
```

```
C      INTEGRATION OF THE FREE ENERGY FT, DEFINED IN
C      SUBPROGRAM FTV, OVER THE VARIOUS K-SPACE REGIONS
DO20 NA=1,NGUU
TT(1)=PI/4.*GP(NA)+PI/4.
TT(2)=PI/4.*GP(NA)+PI*3./4.
WA=PI/24.*GW(NA)
DO23 KT=1,2
T=COS(TT(KT))
CU(2)=AL*2./3.
IF(N4 .EQ. -1) GOTO 19
ITMAX=100
ALM1=1.E-6
IF(U .GT. EUP) ALM2=AL+1.
IF( U.LT.EUP .AND. U .GT. ELO) ALM2=AL
IF( U.LT. ELO) ALM2=AL+1.
CALL ZFALSE(FGO,.0001,5,ALM1,ALM2,P,ITMAX,IER)
CU(2)=P
19  RAY=44.
DO21 NU=1,2
NUU=NU+1
DO22 NB=1,NGU
P=(CU(NUU)-CU(NU))*GP(NB)/2.+(CU(NUU)+CU(NU))/2.
WP=(CU(NUU)-CU(NU))*GW(NB)/2.
FT=FTV(T,P,U,R,V,AD1,AD2,AD3,CC,A)*WP*WA
C1(NU)=C1(NU)+FT
22  CONTINUE
21  CONTINUE
23  CONTINUE
20  CONTINUE
IF( NGG .EQ. -1) GOTO 101
DO34 NU=3,NX
NUU=NU+1
DO31 NB=1,NGU
P=(CU(NUU)-CU(NU))*GP(NB)*.5+(CU(NUU)+CU(NU))* .5
WP=(CU(NUU)-CU(NU))*GW(NB)*.5
TC=ARCOS( (COS(3.*ARCOS((-A*P+U/AD1/2.)/SQRT(P*P+AD2)))*SQRT((
C  P*P+AD2)*(P*P+AD2)*(P*P+AD2))-CC*AD3)/(P*P*P))
DO32 NA=1,NGUU
TT(1)=HP(NA)*TC/2.+TC/2.
WT(1)=HW(NA)*TC/12.
TT(2)=HP(NA)*(3.14159265-TC)/2.+(3.14159265+TC)/2.
WT(2)=HW(NA)*(3.14159265-TC)/12.
DO 33 KT=1,2
T=COS(TT(KT))
FT=FTV(T,P,U,R,V,AD1,AD2,AD3,CC,A)*WP*WT(KT)
C1(NU)=C1(NU)+FT
33  CONTINUE
32  CONTINUE
31  CONTINUE
34  CONTINUE
GO TO 101
102 DO40 NU=1,NX
NUU=NU+1
```



```
DO41 NB=1,NGU
P=(CU1(NUU)-CU1(NU))*GP(NB)*.5+(CU1(NUU)+CU1(NU))* .5
WP=(CU1(NUU)-CU1(NU))*GW(NB)*.5
TC=3.14159265/3.
IF(UXX.EQ.0..OR.NU.GT.1)GOTO70
GOTO71
70 TC=ARCOS(ABS(A-UXX/(2.*AD1*P)))
71 RAY=3.
DO42 NA=1,NGUU
TT(1)=HP(NA)*TC/2.+TC/2.
WT(1)=HW(NA)*TC/2.
TT(2)=HP(NA)*(3.14159265/2.-TC)/2.+(3.14159265/2.+TC)/2.
WT(2)=HW(NA)*(3.14159265/2.-TC)/2.
DO43 KT=1,2
T=COS(TT(KT))
FT=FTO(T,P,UXX,R,AD1,A)*WP*WT(KT)
T1(NU)=T1(NU)+FT
43 CONTINUE
42 CONTINUE
41 CONTINUE
40 CONTINUE
101 GAIL=44.

TOT1(L)=0.
TOT2(L)=0.
DO46 KC=1,13
TOT2(L)=TOT2(L)+T1(KC)+T11(KC)
TOT1(L)=TOT1(L)+C1(KC)+C11(KC)
46 CONTINUE
FR(L)=4./(PI*AA)*(TOT1(L))+U*ANN
FRL(L)=4./(PI*AA)*TOT2(1)+UXX*ANN
50 CONTINUE
WRITE(6,808)(FR(LP),LP=1,7)
WRITE(6,808)(FR(LW),LW=8,14)
WRITE(6,808)(FR(LZ),LZ=15,21)
52 CONTINUE
808 FORMAT(7F9.4)
DATA V2/1.E-12,.0105,.0205,.0305,.0405,.0505,.0605,.0705,.0805,
C .0905,.1005,.1105,.1205,.1305,.1405,.1505,.1605,.1705,.1805,
C .1905,.2005/
DATA R2/1.E-17,.01,.02,.03,.04,.05,.06,.07,.08,.09,.1/
DATA GP/-.9815606,-.904117,-.769902,-.5873179,-.367831,-.125233,
C .125233,-.367831,-.5873179,-.769902,-.904117,-.9815606/
DATA GW/.047175,.106939,.160078,.203167,.2334925,.249147,
C .249147,.233492,.203167,.160078,.106939,.047175/
DATA HP/-.9815606,-.904117,-.769902,-.5873179,-.367831,-.125233,
C .125233,-.367831,-.5873179,-.769902,-.904117,-.9815606/
DATA HW/.047175,.106939,.160078,.203167,.2334925,.249147,
C .249147,.233492,.203167,.160078,.106939,.047175/
STOP
END
FUNCTION FGO(X)
COMMON T,U,V,R,AD1,AD2,AD3,EUP,ELO,CC,A
```

```
IF( V.LT..01) GOTO 10
D2=V*V/AD1/AD1
D3=V*V*V/AD1/AD1/AD1
F=ARCOS( (X*X*X*T/D3+CC)/SQRT( (X*X/D2+1.)*(X*X/D2+1.)*(X*X/D2+1.
C  )) )/3.
GOTO11
10 RAY=4.
F=ARCOS( (X*X*X*T+CC*AD3)/SQRT( (X*X+AD2)*(X*X+AD2)*(X*X+AD2) ) )/3.
11 RAT=4.
IF( U .GT. EUP) GOTO200
IF( U .LT. ELO) GOTO202
FGO=AD1*(A*X+SQRT(X*X+AD2)*(-.5*COS(F)+SQRT(3.)*.5*SIN(F))) -U/2.
GOTO201
200 FGO=AD1*(A*X+SQRT(X*X+AD2)*COS(F)) -U/2.
GOTO201
202 FGO=AD1*(A*X+SQRT(X*X+AD2)*(-.5*COS(F)-SQRT(3.)*.5*SIN(F))) -U/2.
201 RAY=44.
RETURN
END
FUNCTION FTO(T,P,UXX,R,AD1,A)
A2=(AD1*(A*P-P*T)-UXX/2.)/R*2.
A1=(AD1*(A*P+P*T)-UXX/2.)/R*2.
IF(A1 .LT. -14.) F1=R*A1
IF(A1 .GT. 20.) F1=0.
IF(A1 .GT. .0 .AND. A1 .LT. 20.) F1=-R*ALOG(1.+EXP(-A1))
IF(A1 .LT. .0 .AND. A1 .GT. -14.) F1=R*A1-R*ALOG(1+EXP(-ABS(A1)))
IF(A2 .LT. -14.) F2=R*A2
IF(A2 .GT. 20.) F2=0.
IF(A2 .GT. 0. .AND. A2 .LT. 20.) F2=-R*ALOG(1.+EXP(-A2))
IF(A2 .LT. 0. .AND. A2 .GT. -14.) F2=R*A2-R*ALOG(1.+EXP(-ABS(A2)))
FTO=.5*(F1+F2)
RETURN
END
FUNCTION FTV(T,P,U,R,V,AD1,AD2,AD3,CC,A)
F=ARCOS( (P*P*P*T+CC*AD3)/SQRT( (P*P+AD2)*(P*P+AD2)*(P*P+AD2) ) )/3.
DR1=P*P*P*P*(1.-T*T)+3.*P*P*AD2-2.*P*T*CC*AD3+3.*AD2*AD2
DK=(P*T*AD2-CC*AD3)/SQRT( (P*P+AD2)*DR1)
C2=COS(F)
S2=SIN(F)
A1=(AD1*(A*P+SQRT(P*P+AD2)*C2)-U/2.)*2./R
A2=(AD1*(A*P+SQRT(P*P+AD2)*(-.5*C2-SQRT(3.)*.5*S2))-U/2.)*2./R
A3=(AD1*(A*P+SQRT(P*P+AD2)*(-.5*C2+SQRT(3.)*.5*S2))-U/2.)*2./R
IF(A1 .LT. -14.) F1=R*A1
IF(A1 .GT. 20.) F1=0.
IF(A1 .GT. .0 .AND. A1 .LT. 20.) F1=-R*ALOG(1.+EXP(-A1))
IF(A1 .LT. .0 .AND. A1 .GT. -14.) F1=R*A1-R*ALOG(1+EXP(-ABS(A1)))
IF(A2 .LT. -14.) F2=R*A2
IF(A2 .GT. 20.) F2=0.
IF(A2 .GT. 0. .AND. A2 .LT. 20.) F2=-R*ALOG(1.+EXP(-A2))
IF(A2 .LT. 0. .AND. A2 .GT. -14.) F2=R*A2-R*ALOG(1.+EXP(-ABS(A2)))
IF(A3 .LT. -14.) F3=R*A3
IF(A3 .GT. 20.) F3=0.
IF( A3 .GT. 0. .AND. A3 .LT. 20.) F3=-R*ALOG(1.+EXP(-A3))
```

```
IF (A3 .LT. 0. .AND. A3 .GT. -14.) F3=P*A3-R*ALOG(1.+EXP(-ABS(A3)))  
FTV=F1+F2+F3  
RETURN  
END
```

```
/*
```

```
//GO.SYSIN DD *
```

```
//ACXGKSIN JOB (****,****),SCOTT,MSGCLASS=R
//FORTRAN EXEC FORTGCG
DIMENSION FR(1386),TOT6(40),TOT4(40),TOT7(40),ILP(40)
DIMENSION V2(22),R2(12)
DIMENSION AA(3,3),BB(3),XX(3),HH(3),IP(3)
DIMENSION SC(40),TOTAL(21,11,6)
DIMENSION R3(6,6,11),V3(6,6,11),U3(6,6,11),U4(1386)
C FREE ENERGY AND CHEMICAL POTENTIAL VALUES CALCULATED
C IN SEPARATE PROGRAM CONSTITUTE INPUTED DATA
DO 10 JR=1,198
J1=(JR-1)*7+1
J2=J1+6
READ(5,90) (FR(J),J=J1,J2)
10 CONTINUE
90 FORMAT(7F9.4)
DO 70 JR=1,198
J1=(JR-1)*7+1
J2=J1+6
READ(5,71) (U4(JX),JX=J1,J2)
70 CONTINUE
71 FORMAT(7F8.5)
W1S=(82.*82.+44.*44.+2.*(65.*65.+50.*50.))/6.
W2S=38.*38.
WC=-6
W=1.E-11
C FOR A GIVEN ELECTRON CONCENTRATION (NN), COUPLING
C PARAMETER (LC) AND TEMPERATURE (K), THE CORRESPONDING
C ELECTRONIC GAP (V) AND CHEMICAL POTENTIAL (U) ARE
C CALCULATED FROM INPUTED FREE ENERGY AND CHEMICAL
C POTENTIAL DATA BY FITTING THE FREE ENERGY TO A
C QUADRATIC IN THE VICINITY OF THE MINIMUM
DO 11 NN=1,6
DO 49 LC=1,6
DO 12 K=1,11
R3(NN,LC,K)=R2(K)
IF(K.EQ.1) VV=1000.
DO 13 L=1,21
V=V2(L)
R=R2(K)
LX1=(NN-1)*231+(K-1)*21+1
LX=(NN-1)*231+(K-1)*21+L
E1=((W1S-W2S)*V*V/VV/VV+W2S+V/VV*(82.*82.-W1S))
E2=((W1S-W2S)*V*V/VV/VV+W2S+V/VV*(44.*44.-W1S))
E3=((W1S-W2S)*V*V/VV/VV+W2S+V/VV*(65.*65.-W1S))
E4=((W1S-W2S)*V*V/VV/VV+W2S+V/VV*(50.*50.-W1S))
E5=SQRT(W2S)/(80.65*WC*R)
FPH=0.
TOT6(L)=-20.-.1*L
TOTAL(L,K,LC)=TOT6(L)
IF(K.EQ.1) GOTO 18
IF(E1.LT.0..OR.E2.LT.0..OR.E3.LT.0..OR.E4.LT.0.) GOTO13
E1=SQRT(E1)/(80.65*WC*R)
E2=SQRT(E2)/(80.65*WC*R)
```

```
E3=SQRT(E3)/(80.65*WC*R)
E4=SQRT(E4)/(80.65*WC*R)
PPH=W*R*(ALOG((1.-EXP(-E1))*(1.-EXP(-E2))*(1.-EXP(-E3))*
C (1.-EXP(-E3))*(1.-EXP(-E4))*(1.-EXP(-E4))))
C -6.*ALOG(1.-EXP(-E5)))
18 SHELL=4.
TOT6(L)=V*V*SC(LC)/100.+FR(LX)-FR(LX1)+PPH
TOTAL(L,K,LC)=TOT6(L)
13 CONTINUE
LP=1
XP=TOT6(1)
DO 50 LL=2,21
IF(TOT6(LL).LT.XP) LP=LL
IF(TOT6(LL).LT.XP) XP=TOT6(LL)
50 CONTINUE
V3(NN,LC,K)=0.
IF(LP.EQ.21) V3(NN,LC,K)=20.
ILP(K)=LP
IF(LP.EQ.1.OR.LP.EQ.21) U3(NN,LC,K)=40.
IF(LP.EQ.1.OR.LP.EQ.21) GOTO 51
DO 33 I=1,3
J=LP+I-2
AA(I,1)=1.
AA(I,2)=V2(J)
AA(I,3)=V2(J)*V2(J)
BB(I)=TOT6(J)
33 CONTINUE
IA=3
MM=3
NK=3
TOT=0.0
KBAS=3
C LEAST SQUARE PROGRAM FITS FREE ENERGY TO A QUADRATIC
C IN THE VICINITY OF THE LOCAL MINIMUM
CALL LLSQP(AA,IA,MM,NK,BB,TOT,KBAS,XX,HH,IP,IER)
V3(NN,LC,K)=-XX(2)/(2.*XX(3))
LUU=(NN-1)*231+(K-1)*21+LP
LU1=LUU-1
IF(V3(NN,LC,K).GT.V2(LP)) LU1=LUU+1
U3(NN,LC,K)=U4(LUU)+ABS(V3(NN,LC,K)-V2(LP))*(U4(LU1)-U4(LUU))
51 FRAN=4.
IF(K.GT.1) GO TO 12
IF(LP.NE.1.AND.LP.NE.21) VV=V3(NN,LC,K)
12 CONTINUE
C THE TRANSITION TEMPERATURE AND CORRESPONDING ELECTRONIC
C GAP FOR A GIVEN NN AND LC ARE CALCULATED
LTE=99
DO 300 J=1,10
JJ=J+1
IF(ILP(J).NE.1.AND.ILP(JJ).EQ.1) LTE=J
300 CONTINUE
IF(LTE.EQ.99) GO TO 48
NL=ILP(LTE)+1
```

```
DO 302 MT=1,8
DO 303 JX=1,NL
LTZ=LTE+1
TOT7(JX) = (TOTAL(JX,LTE,LC) - TOTAL(1,LTE,LC)) + (TOTAL(JX,LTZ,LC) -
303 C TOTAL(1,LTZ,LC) - TOTAL(JX,LTE,LC) + TOTAL(1,LTE,LC)) * (MT-1) / 7.
CONTINUE
LP2=1
XTT=TOT7(1)
DO 304 JS=2,NL
IF(TOT7(JS) .LT. XTT) LP2=JS
304 IF(TOT7(JS) .LT. XTT) XTT=TOT7(JS)
CONTINUE
IF(LP2 .EQ. 1) GO TO 302
DO 306 JG=1,3
JA=LP2+JG-2
AA(JG,1)=1.
AA(JG,2)=V2(JA)
AA(JG,3)=V2(JA)*V2(JA)
306 BB(JG)=TOT7(JA)
CONTINUE
IA=3
MM=3
NK=3
TOT=0.0
KBAS=3
CALL LLSQF(AA,IA,MM,NK,BB,TOT,KBAS,XY,HH,IP,IER)
ZG=-XY(2)/(2.*XX(3))
TEM=LTE*1.+(MT-1)/7.-1.
LUU=(NN-1)*231+(LTE-1)*21+LP2
LU1=LUU+1
IF(ZG .LT. V2(LP2)) LU1=LUU-1
LU2=LUU+21
LU3=LU2+1
IF(ZG .LT. V2(LP2)) LU3=LU2-1
UG=U4(LUU)+ABS(ZG-V2(LP2))*(U4(LU1)+(U4(LU3)-U4(LU1)))*
302 C (MT-1)/7.-(U4(LUU)+(U4(LU2)-U4(LUU))*(MT-1)/7.))
CONTINUE
KH=LTE+1
R3(NN,LC,KH)=TEM
KH1=KH+1
IF(NN .NE. 1 .AND. KH1 .LT. 12) R3(NN,LC,KH1)=TEM
U3(NN,LC,KH)=UG
IF(NN .EQ. 1) U3(NN,LC,KH)=1.E-10
LUU=(NN-1)*231+(LTE-1)*21+1
LU1=LUU+1
IF(ZG .LT. V2(LP2)) LU1=LUU-1
LU2=LUU+21
LU3=LU2+1
IF(ZG .LT. V2(LP2)) LU3=LU2-1
UG=U4(LUU)+ABS(ZG-V2(LP2))*(U4(LU1)+(U4(LU3)-U4(LU1)))*
C (TEM-(LTE-1)*1.)-(U4(LUU)+(U4(LU2)-U4(LUU))*(TEM-(LTE-1)*1.))
IF(NN .NE. 1 .AND. KH1 .LT. 12) U3(NN,LC,KH1)=UG
V3(NN,LC,KH)=ZG
```

```
IF ( NN .EQ. 1) V3(NN,LC,KH)=0.
48  FRAN=4.
    WRITE(6,446) (V3(NN,LC,K9),K9=1,7)
    WRITE(6,447) (V3(NN,LC,K6),K6=8,11)
    WRITE(6,446) (U3(NN,LC,K8),K8=1,7)
    WRITE(6,447) (U3(NN,LC,K4),K4=8,11)
    WRITE(6,446) (R3(NN,LC,N4),N4=1,7)
    WRITE(6,447) (R3(NN,LC,N5),N5=8,11)
447  FORMAT(4F8.4)
446  FORMAT(7F8.4)
49   CONTINUE
11   CONTINUE
    DATA V2/1.F-7,1.05,2.05,3.05,4.05,5.05,6.05,7.05,8.05,
C 9.05,10.05,11.05,12.05,13.05,14.05,15.05,16.05,17.05,
C 18.05,19.05,20.05/
    DATA R2/1.E-11,1.,2.,3.,4.,5.,6.,7.,8.,9.,10.,11./
    DATA SC/2.2,2.4,2.6,2.7,2.8,3.0/
    STOP
    END
//GO.SYSIN DD *
```

REFERENCES

1. J.A. Wilson, F.J. DiSalvo, S. Mahajan, Adv. in Physics 24, 117 (1975).
2. R.E. Peierls, Quantum Theory of Solids, Oxford University Press.
3. H. Frohlich, Proc. Roy. Soc. A223, 296 (1954).
4. N.J. Doran, Physica 99B, 227 (1980).
5. J.A. Wilson, A.D. Yoffe, Adv. in Phys. 18, 193 (1969).
6. L.F. Mattheiss, Phy. Rev. B8, 3719 (1973).
7. J.E. Inglesfield, J. Phys. C. 13, 17 (1980).
8. G. Wexler, A.M. Woolley, J. Phys. C. 9, 1185 (1976).
9. T.M. Rice, G.K. Scott, Phy. Rev. Lett. 35, 120 (1975).
10. S.K. Chan, V. Heine, J. Phys. F. 3, 795 (1973).
11. W.L. McMillan, Phys. Rev. B16, 643 (1977).
12. J.M. Ziman, Electrons and Phonons, Oxford University Press (1960).
13. D.E. Moncton, J.D. Axe, F.J. DiSalvo, Phys. Rev. Lett. 34, 734 (1975).
14. A.B. Migdal, Sov. Phys.-JETP 7, 996 (1958).
15. J.A. Holy, M.V. Klein, W.L. McMillan, S.F. Meyer, Phys. Rev. Lett. 37, 1145 (1976).
16. W. Kohn, Phys. Rev. Lett. 2, 393 (1959).
17. W.M. Lomer, Proc. Phys. Soc. (London) 80, 489 (1962).
18. J.E. Graebner, Solid State Commun, 21, 353 (1977).
19. P.A. Lee, T.M. Rice, P.W. Anderson, Solid State Commun. 14, 703 (1974).



20. A.S. Barker, Jr., J.A. Ditzenberger, F.J. DiSalvo, Phys. Rev. B 12, 2049 (1975).
21. R.H. Craven, S.F. Meyer, Phys. Rev. B 16, 4583 (1977).
22. E.F. Steigmeier, G. Harbeke, H. Auderset, F.J. DiSalvo, Solid State Commun. 20, 667 (1976).
23. J.C. Irwin, Private Communication, March, 1981
24. N.H.S. Lee, M. Garcia, H. McKinzie, A. Wold, J. Solid State Chem. 1, 190 (1970).
25. D.J. Huntley, R.F. Frindt, Can. J. Phys. 52, 861 (1974)
26. J.A. Wilson, Phys. Rev. B 15, 5748 (1977).